

Oligarchic growth of giant planets

E. W. Thommes

*Astronomy Department, 601 Campbell Hall, University of California, Berkeley, California
94720*

thommes@astro.berkeley.edu

M. J. Duncan

Physics Department, Queen's University, Kingston, Ontario K7L 3N6

H. F. Levison

Southwest Research Institute, 1050 Walnut Street, Suite 426, Boulder, Colorado 80302

ABSTRACT

Runaway growth ends when the largest protoplanets dominate the dynamics of the planetesimal disk; the subsequent self-limiting accretion mode is referred to as “oligarchic growth.” Here, we begin by expanding on the existing analytic model of the oligarchic growth regime. From this, we derive global estimates of the planet formation rate throughout a protoplanetary disk. We find that a relatively high-mass protoplanetary disk ($\sim 10\times$ minimum-mass) is required to produce giant planet core-sized bodies ($\sim 10 M_{\oplus}$) within the lifetime of the nebular gas ($\lesssim 10$ million years). However, an implausibly massive disk is needed to produce even an Earth mass at the orbit of Uranus by 10 Myrs. Subsequent accretion without the dissipational effect of gas is even slower and less efficient. In the limit of non-interacting planetesimals, a reasonable-mass disk is unable to produce bodies the size of the Solar System’s two outer giant planets at their current locations on *any* timescale; if collisional damping of planetesimal random velocities is sufficiently effective, though, it may be possible for a Uranus/Neptune to form in situ in less than the age of the Solar System. We perform numerical simulations of oligarchic growth with gas, and find that protoplanet growth rates agree reasonably well with the analytic model as long as protoplanet masses are well below their estimated final masses. However, accretion stalls earlier than predicted, so that the largest final protoplanet masses are smaller than those given by the model. Thus the oligarchic growth model, in the form developed here, appears to provide an upper limit for the efficiency of giant planet formation.

Subject headings: Accretion — extrasolar planets — Jovian planets — origin,
Solar System — planetary formation

1. Introduction

The initial growth mode in a disk of accreting planetesimals is runaway growth (eg. Wetherill and Stewart 1989, Kokubo and Ida 1996), wherein the mass doubling time for the largest bodies is the shortest. However, when these runaway bodies, or protoplanets, become sufficiently massive, it is their gravitational scattering (often called viscous stirring) which dominates the random velocity evolution of the background planetesimals, rather than the interactions among the planetesimals. Since the accretion cross-section of a protoplanet is smaller among planetesimals with higher random velocities, protoplanet growth now switches to a slower, self-limiting mode, in which the mass ratio of any two protoplanets at adjacent locations in the disk approaches unity over time. Ida and Makino (1993) investigated this transition analytically and through N-body simulations, and Kokubo and Ida (1998, 2000, 2002) studied the subsequent accretion mode, giving it the name “oligarchic growth”. In the terrestrial region, the final accretion phase likely consisted of the merging of oligarchically-accreted protoplanets; simulations show that such a process fairly readily produces bodies with masses comparable to present-day terrestrial planets (eg. Chambers and Wetherill 1998). However, an analogous phase in the trans-Saturnian region would have been highly inefficient; even sub-Earth mass protoplanets excite each other to high random velocities on a timescale short compared to their collision timescale, so that only negligible accretion occurs (Levison and Stewart 2001). Thus, it appears that oligarchic growth alone must be called upon to account for almost all accretional growth in the outer Solar System.

In Section 2, we examine the condition for crossover from runaway to oligarchic growth, and show that this transition is expected to set in when the largest bodies are still several orders of magnitude below an Earth mass. In Section 3, we summarize the previous work on oligarchic growth timescale estimates, obtain a protoplanet mass function, then extend the model by considering a system in which the planetesimal surface density varies in a self-consistent way. We show that with an approximately tenfold increase in surface density relative to the minimum-mass model, protoplanets of mass $\sim 10 M_{\oplus}$ can form. The standard nucleated instability model of gas giant formation, wherein a massive gas envelope accumulates onto a solid core during the nebular gas lifetime ($\lesssim 10$ million years, e.g. Strom, Edwards and Skrutskie 1990), is thought to require bodies of this mass (Mizuno et al 1978, Pollack et al 1996). Our estimate of the required density enhancement is somewhat higher than that of Weidenschilling (1998), who finds, using a multizone statistical simulation, that

$4\times$ the minimum mass is insufficient to produce giant planet cores, but that an additional “modest increase” is sufficient to make it happen.

The formation of “ice giant” planets like Uranus and Neptune at stellocentric distances of $\gtrsim 20$ AU cannot be similarly accounted for during this time. In Section 5, we discuss the validity of the model. In Section 6, we obtain oligarchic growth rate estimates in the absence of gas, to ascertain how much more accretion could have taken place subsequent to the removal of the nebular gas. We consider two extremes: that of collisionless planetesimals, and that of maximally effective collisional damping of random velocities (though without fragmentation). In the former limit, Uranus- and Neptune-mass planets cannot be produced at their current locations on any timescale unless the initial protoplanetary disk is implausibly massive; in the latter limit, such planets might be formed in a reasonable-mass disk and in less than the age of the Solar System.

In Section 7, we test the semianalytic predictions for the pre-gas dispersal phase of oligarchic growth against numerical simulations. We find good agreement as long as protoplanet masses are well below their theoretical final masses, however growth in the simulations stalls early, so that the final masses fall short of those predicted by the model. We summarize the results and discuss implications in Section 8.

2. Transition to oligarchic growth

Ida and Makino (1993) derive the following condition for the dominance of protoplanet-planetesimal scattering over planetesimal-planetesimal scattering in determining the random velocity evolution of the planetesimal disk:

$$2\Sigma_M M > \Sigma_m m, \quad (1)$$

where M and m are the protoplanet mass and the effective planetesimal mass, respectively, Σ_m is the surface mass density of the planetesimal disk, and Σ_M is the effective surface density of a protoplanet in the disk. The latter is given by

$$\Sigma_M = \frac{M}{2\pi a \Delta a_{\text{stir}}} \quad (2)$$

where a is the semimajor axis of the protoplanet, and Δa_{stir} is the width of the annulus within which the disk is gravitationally stirred by the protoplanet. For a single protoplanet, this width is about $5.2a\langle e_m^2 \rangle^{1/2}$, where $\langle e_m^2 \rangle^{1/2}$ is the RMS eccentricity of planetesimals in the disk. Hereafter, we shorten the notation to e_m , and likewise we write $\langle i_m^2 \rangle^{1/2}$ as i_m . This width is set by the conservation of the Jacobi energy of planetesimals relative to the

protoplanet; details are given in Ida and Makino (1993). A simplification inherent in this approach, and one we shall make use of throughout, is the representation of the planetesimals as a population of uniform-mass bodies. As discussed by Ida and Makino (1993), the effective mass is the RMS mass of the full distribution. This requires that e_m and i_m depend only weakly on m . As we shall see below (Eq. 10), this is indeed the case. At the same time, though, one should bear in mind that the planetesimal mass spectrum will span many orders of magnitude; as an example, 1 to 100 km radii correspond to a mass range of 10^{-12} to $10^{-6} M_\oplus$. The effect of planetesimal sizes on accretion is considered in Section 4.

When a disk is stirred by multiple protoplanets, one must account for the overlap of stirred annuli. One can do this in an average way by taking

$$\Delta a = \text{Min}(5.2ae, \Delta a_{\text{proto}}), \quad (3)$$

where Δa_{proto} is the characteristic spacing of protoplanet orbits. Kokubo and Ida (1998) find that adjacent protoplanets in a swarm of planetesimals keep a typical separation of a fixed number b of Hill radii, with $b \sim 10$. The Hill radius of a body of mass M and semimajor axis a orbiting a primary of mass M_* is defined as

$$r_{\text{H}} = \left(\frac{M}{3M_*} \right)^{1/3} a \equiv h_M a, \quad (4)$$

where h_M is the reduced Hill radius. Dispersion-dominated random velocities means that $e \gtrsim 2h$, so that $10r_{\text{H}} < 5.2ae$, and thus we use $\Delta a = 10r_{\text{H}}$ throughout. From Eqs. 1 and 2, the protoplanet mass at which oligarchic growth commences is then

$$\begin{aligned} M_{\text{oli}} &\sim \frac{1.6a^{6/5}b^{3/5}m^{3/5}\Sigma_m^{3/5}}{M_*^{1/5}} \\ &\sim 2.1 \times 10^{-6} \left(\frac{b}{10} \right)^{3/5} \left(\frac{M_*}{M_\odot} \right)^{-1/5} \left(\frac{\Sigma_m}{30\text{g/cm}^2} \right)^{3/5} \left(\frac{m}{10^{-9}M_\oplus} \right)^{3/5} \left(\frac{a}{1\text{AU}} \right)^{(6-2k)/5} M_\oplus \end{aligned} \quad (5)$$

For the case of an isolated protoplanet ($b \sim 35 - 55$) growing in a swarm of $m = 10^{23} - 10^{24}$ g (200-400 km radius) planetesimals, Ida and Makino (1993) calculate $M_{\text{oli}} \sim 10^{-3} - 10^{-2} M_\oplus$. Considering a population of planetesimals ($b \sim 10$; see above), and using a perhaps more realistic (eg. Lissauer 1987) planetesimal mass of 10^{19} g (~ 10 km) one obtains even lower crossover masses. Fig. 1 shows M_{oli} throughout the protoplanetary disk for a one and ten times minimum-mass nebula (Hayashi 1981; see Eqs. 15 and 17 below) with 10 km planetesimals. M_{oli} is a few $\times 10^{-5} M_\oplus$ or less. Thus, although runaway growth is much more rapid than oligarchic growth, it ceases long before protoplanets approaching an Earth mass can form. For this reason, the contribution to a planet's formation timescale from oligarchic growth is much more important than that from runaway growth, and we neglect the latter in our analysis.

3. Oligarchic growth rate estimates

When planetesimal random velocities are dispersion-dominated rather than shear-dominated, the mass accretion rate of an embedded protoplanet is well described by the particle-in-a-box approximation (Safronov 1969, Wetherill 1980, Ida and Nakazawa 1989):

$$\frac{dM}{dt} \simeq F \frac{\Sigma_m}{h} \pi R_M^2 \left(1 + \frac{v_{\text{esc}}^2}{v_{\text{rel}}^2} \right) v_{\text{rel}}, \quad (6)$$

where h the disk scale height, R_M the protoplanet radius, v_{esc} the escape velocity from the protoplanet's surface, and v_{rel} the characteristic relative velocity between the protoplanet and the planetesimals. F is a factor which compensates for the underestimation of the growth rate which results from using the RMS value of the planetesimal random velocity for v_{rel} ; its value is ~ 3 (Greenzweig and Lissauer 1992). We apply the following approximations: $h \simeq ai_m$, $i_m \simeq e_m/2$, $v_{\text{esc}}^2/v_{\text{rel}}^2 \gg 1$, and $v_{\text{rel}} \simeq e_m a \Omega$, where Ω is the Keplerian frequency. These are valid if gravitational focusing and dynamical friction are both effective; see for example Kokubo and Ida (1996) for details. The above equation can then be rewritten as

$$\frac{dM}{dt} \simeq \frac{C \Sigma_m M^{4/3}}{e_m^2 a^{1/2}} \quad (7)$$

with $C = 6\pi^{2/3}[3/(4\rho_M)]^{1/3}[G/M_*]^{1/2}$, where ρ_M is the bulk density of a protoplanet.

The planetesimals attain an equilibrium RMS eccentricity, e_m^{eq} , when gravitational perturbations due to the protoplanets are balanced by dissipation due to gas drag. Following Ida and Makino (1993), we obtain e_m^{eq} by equating the viscous stirring timescale due to a protoplanet of mass M , T_{VS}^{M-m} , with the eccentricity damping timescale due to gas drag for planetesimals of characteristic mass m , $T_{\text{gas}}^{e_m}$. The former is given by

$$T_{\text{VS}}^{M-m} \simeq \frac{1}{40} \left(\frac{\Omega^2 a^3}{GM} \right)^2 \frac{e_m^4}{n_{sM} a^2 \Omega} \quad (8)$$

(Ida 1990, Ida and Makino 1993), where n_{sM} is the surface number density of protoplanets, Σ_M/M .

The gas drag eccentricity damping timescale is given by

$$T_{\text{gas}}^{e_m} \simeq \frac{1}{e_m} \frac{m}{(C_D/2)\pi r_m^2 \rho_{\text{gas}} a \Omega} \equiv \frac{T_{\text{gas}}}{e_m} \quad (9)$$

(Adachi, Hayashi and Nakazawa 1976). C_D is a dimensionless drag coefficient, of order 1 for spherical planetesimals of mass $10^{18} - 10^{24}$ g, r_m is the radius of a planetesimal, and ρ_{gas} is the gas volume density.

Setting $T_{\text{VS}}^{M-m} = T_{\text{gas}}^{e_m}$ and solving for e_m , one obtains

$$\begin{aligned}
 e_m^{\text{eq}} (\simeq 2i_m^{\text{eq}}) &\simeq \frac{1.7m^{1/15} M^{1/3} \rho_m^{2/15}}{b^{1/5} C_D^{1/5} \rho_{\text{gas}}^{1/5} M_*^{1/3} a^{1/5}} \\
 &\simeq 0.04 \left(\frac{b}{10}\right)^{-1/5} \left(\frac{M_*}{M_\odot}\right)^{-1/3} \left(\frac{\rho_{\text{gas}}(1\text{AU})}{1.4 \times 10^{-9} \text{g/cm}^3}\right)^{-1/5} \left(\frac{m}{10^{-9} M_\oplus}\right)^{1/15} \\
 &\times \left(\frac{a}{1\text{AU}}\right)^{(\alpha-1)/5} \left(\frac{M}{1M_\oplus}\right)^{1/3}
 \end{aligned} \tag{10}$$

where ρ_m is the planetesimal bulk density and the gas density is a power law, $\rho_{\text{gas}} \propto a^{-\alpha}$.

Substituting Eq. 10 into Eq. 7, one gets an estimate for the oligarchic-regime growth rate:

$$\frac{dM}{dt} \simeq \frac{3.9b^{2/5} C_D^{2/5} G^{1/2} M_*^{1/6} \rho_{\text{gas}}^{2/5} \Sigma_m}{\rho_m^{4/15} \rho_M^{1/3} a^{1/10} m^{2/15}} M^{2/3} \tag{11}$$

As a check on the validity of using $e_m = e_m^{\text{eq}}$ in calculating the accretion rate of protoplanets, one can compare T^{e_m} , the timescale to reach e_m^{eq} (obtained from Eq. 10 and Eq. 8 or 9), to the growth timescale,

$$T_{\text{grow}} \equiv \frac{M}{dM/dt}. \tag{12}$$

Using power law gas and solids densities, $\rho_{\text{gas}} \propto a^{-\alpha}$ and $\Sigma_m \propto a^{-k}$, and setting $C_D = 1$, $\rho_m = \rho_M = 1.5 \text{ g/cm}^3$, one obtains

$$\begin{aligned}
 \frac{T^{e_m}}{T_{\text{grow}}} &\simeq 10^{-2} \left(\frac{m}{10^{-9} M_\oplus}\right)^{2/15} \left(\frac{\Sigma_m(1 \text{ AU})}{30 \text{g/cm}^2}\right) \left(\frac{\rho_{\text{gas}}(1 \text{ AU})}{1.4 \times 10^{-9} \text{g/cm}^3}\right)^{-2/5} \\
 &\times \left(\frac{M}{1 M_\oplus}\right)^{-2/3} \left(\frac{a}{1 \text{ AU}}\right)^{(11-4\alpha)/15-k}
 \end{aligned} \tag{13}$$

For a nebula of ten times the minimum mass or less (see below), this is less than one when the protoplanet mass M is a few $\times 10^{-2} M_\oplus$ or larger.

Kokubo and Ida (2000) calculate T_{grow} at the heliocentric distances of each of the giant planets in the Solar System. But one can also directly solve the above differential equation for the protoplanet mass:

$$\begin{aligned}
 M &\simeq \left(\frac{1.3b^{2/5} C_D^{2/5} G^{1/2} M_*^{1/6} \rho_{\text{gas}}^{2/5} \Sigma_m}{\rho_m^{4/15} \rho_M^{1/3} a^{1/10} m^{2/15}} t + M_0^{1/3} \right)^3 \\
 &\simeq \left[\left(\frac{0.15}{1M_\oplus}\right)^{1/3} \left(\frac{\rho_{\text{gas}}(1\text{AU})}{1.4 \times 10^{-9} \text{g/cm}^2}\right)^{2/5} \left(\frac{m}{10^{-9} M_\oplus}\right)^{-2/15} \left(\frac{a}{1\text{AU}}\right)^{-1/10-2\alpha/5-k} \right. \\
 &\quad \left. \times \left(\frac{\Sigma_m(1\text{AU})}{30 \text{g/cm}^2}\right) \left(\frac{t}{10^5 \text{yrs}}\right) + M_0^{1/3} \right]^3,
 \end{aligned} \tag{14}$$

where we have taken $b = 10$, $\rho_M = \rho_M = 1.5 \text{ g/cm}^3$, $C_D=1$, and $M_* = M_\odot$ in the second line. In this way, one obtains an estimate of the mass of protoplanets throughout the disk at any given time. Examples are shown in Fig. 2, which plots protoplanet mass versus semimajor axis at various times. The calculation is performed using a surface density of solids based on the minimum-mass model of Hayashi (1981):

$$\begin{aligned}\Sigma_m^{\min} &= 7.1(a/1 \text{ AU})^{-3/2} \text{ g/cm}^2, & a < 2.7 \text{ AU} \\ &= 30(a/1 \text{ AU})^{-3/2} \text{ g/cm}^2, & a > 2.7 \text{ AU}\end{aligned}\tag{15}$$

where the discontinuity at 2.7 AU is due to the formation of water ice at that heliocentric distance (the “snow line”). In reality this boundary may have been significantly less sharply defined. Likewise, the snow line’s location is quite uncertain; other models place it around 6 AU (Boss 1995) or 1 AU (Sasselov and Lecar 2000), and it was likely not stationary as the disk and its temperature profile evolved over time. In our model disk, we spread the snow line discontinuity over a radial distance of about 1 AU:

$$\Sigma_m = \left\{ 7.1 + (30 - 7.1) \left[\frac{1}{2} \tanh \left(\frac{a - 2.7 \text{ AU}}{0.5 \text{ AU}} \right) + \frac{1}{2} \right] \right\} \left(\frac{a}{1 \text{ AU}} \right)^{-3/2}\tag{16}$$

For the gas component of the disk, we use the midplane value of the minimum-mass density; this is given by

$$\rho_0^{\min}(r) = 1.4 \times 10^{-9} (r/1 \text{ AU})^{-11/4} \text{ g/cm}^3,\tag{17}$$

The full three-dimensional gas density is of the form

$$\rho(r, z) = \rho_0(r) \exp\{-z^2/z_0(r)^2\} \text{ g/cm}^3,\tag{18}$$

where the disk half-thickness, determined by the balance between the central star’s gravity and the gas pressure gradient in the vertical direction, is

$$z_0(r) = 0.0472 (r/1 \text{ AU})^{5/4} \text{ AU}\tag{19}$$

Fig. 2 shows a “front” of protoplanet growth sweeping outward through the disk over time. The front is quite steep, due principally to the strong dependence of the protoplanet mass on the planetesimal surface density ($M \propto \Sigma_m^3$). For the same reason, the discontinuity in the surface density produces a large jump in the protoplanet masses, so that there is in effect a second, superimposed growth front which is launched at the snow line.

Since the surface density is taken as time-invariant in this estimate, the protoplanet mass everywhere in the disk increases without bound for increasing time. This is of course

unphysical; in reality the growth of the protoplanets will be constrained by the total amount of solids in the disk. At a given location in the disk, the planetesimal surface density will change over time due to depletion of planetesimals by accretion, and due to the systematic radial motion of planetesimals caused by nebular gas drag. To obtain an estimate of the former effect, we begin by assuming a series of protoplanets spaced by $\Delta a = br_H$ (see Section 2). One can estimate the planetesimal surface density in an annulus centered on each one:

$$\begin{aligned}\Sigma_m &= \Sigma_m^0 - \frac{M}{2\pi abr_H} \\ &= \Sigma_m^0 - \frac{(3M_*)^{1/3} M^{2/3}}{2b\pi a^2},\end{aligned}\tag{20}$$

where Σ_m^0 is the original planetesimal surface density at that location. Setting $\Sigma_m = 0$ also gives us a limiting protoplanet mass, at which growth stops because the surface density within Δa drops to zero:

$$M_{\text{lim}} = \frac{2\sqrt{2}[b\pi\Sigma_m^0]^{3/2}a^3}{\sqrt{3M_*}}\tag{21}$$

This is simply the isolation mass (eg. Lissauer 1987; note that our b is a factor of two larger than the B in his Eq. 11), modified as in Kokubo and Ida (1998, 2000) for the case of a population of planetesimals, so that b is determined by the orbital spacing of protoplanets rather than by the gravitational reach of a single protoplanet.

Differentiating Eq. 20, one gets the relationship between the surface density and protoplanet mass rates of change:

$$\left.\frac{\partial\Sigma_m}{\partial t}\right|_{\text{accr}} = \frac{-M_*^{1/3}}{3^{2/3}b\pi a^2 M^{1/3}} \frac{dM}{dt}.\tag{22}$$

In the limit of no planetesimal migration, the behaviour of the system is obtained by substituting Eq. 20 into Eq. 11:

$$\frac{dM}{dt} \simeq AM^{2/3}(\Sigma_m^0 - BM^{2/3})\tag{23}$$

with

$$A = \frac{3.9b^{2/5}C_D^{2/5}G^{1/2}M_*^{1/6}\rho_{\text{gas}}^{2/5}}{\rho_m^{4/15}\rho_M^{1/3}a^{1/10}m^{2/15}}, \quad B = \frac{.23M_*^{1/3}}{ba^2}$$

Solving this differential equation for the protoplanet mass yields

$$M \simeq \left(\frac{\Sigma_m^0}{B}\right)^{3/2} \tanh \left[\left(\frac{1}{3}A\Sigma_m^0\right)^{1/2} B^{1/2} t + \tanh^{-1}(M_0^{1/3} B^{1/2} \Sigma_m^0^{-1/2}) \right]^3\tag{24}$$

However, to obtain a self-consistent description of the coupled evolution of the proto-planet masses and the planetesimal disk in the presence of nebular gas, we must also take into account the planetesimals’ orbital decay. The rate of change of a planetesimal’s semimajor axis under the action of gas drag is given by

$$\left. \frac{da}{dt} \right|_m \simeq -2 \frac{a}{T_{\text{gas}}} \left(\frac{5}{8} e_m^2 + \frac{1}{2} i_m^2 + \eta^2 \right)^{1/2} \left\{ \eta + \left(\frac{\alpha}{4} + \frac{5}{16} \right) e_m^2 + \frac{1}{8} i_m^2 \right\} \equiv v_m \quad (25)$$

(Adachi, Hayashi and Nakazawa 1976). T_{gas} is defined in Eq. 9 (note that $T_{\text{gas}}^{e_m}$ differs from T_{gas} by a factor of $1/e_m$), α as before gives the exponential a -dependence of the gas density, and

$$\eta \equiv \frac{v_{\text{K}} - v_{\text{gas}}}{v_{\text{K}}} = \frac{\pi}{16} (\alpha + \beta) \left(\frac{c_s}{v_{\text{K}}} \right)^2 \quad (26)$$

is the fractional difference between the gas velocity v_{gas} and the local Keplerian velocity v_{K} arising from the partial pressure support of the gas disk; c_s is the sound speed, β gives the exponential a -dependence of the temperature profile ($T \propto a^{-\beta}$), and $c_s/v_{\text{K}} \simeq z_0(r)/r$. Since the rate of orbital decay grows with planetesimal eccentricity and inclination, one can expect this effect to play an increasingly important role as protoplanets grow larger (Eq. 10).

Applying continuity, the rate of change of the surface density at a given radius a in the planetesimal disk due to planetesimal migration alone is

$$\left. \frac{\partial \Sigma_m}{\partial t} \right|_{\text{migr}} = -\frac{1}{a} \frac{\partial}{\partial a} (a \Sigma_m v_m). \quad (27)$$

Using $i_m = e_m/2$, $e_m = e_m^{\text{eq}}$ in Eq. 25, we get v_m as a function of a and $M(a)$. We can then write the equation of continuity as

$$\left. \frac{\partial \Sigma_m}{\partial t} \right|_{\text{migr}} = -\frac{1}{a} \left[\Sigma_m v_m + a v_m \frac{\partial \Sigma_m}{\partial a} + a \Sigma_m \left(\frac{\partial v_m}{\partial a} + \frac{\partial v_m}{\partial M} \frac{\partial M}{\partial a} \right) \right]. \quad (28)$$

Implicit in this treatment is the assumption that the net orbital decay rate of the planetesimals is not significantly affected by the presence of the protoplanets. Tanaka and Ida (1997) performed numerical simulations of protoplanets embedded in a swarm of planetesimals, and found that a protoplanet shepherds planetesimals outside its orbit, even when mutual perturbations among the planetesimals are strong enough to prevent resonant trapping. This shepherding effect arises due to the (approximate) conservation of the planetesimals’ Jacobi energy relative to the protoplanet. However, they also found that once protoplanets are spaced by 15 Hill radii or less, adjacent protoplanets’ contours of constant Jacobi energy overlap too much and shepherding no longer occurs. Since Δa_{proto} is closer to $10 r_{\text{H}}$ for a population of protoplanets embedded in a planetesimal disk (see Section 2), shepherding is unlikely to play much of a role.

The full oligarchic growth model is thus described by a coupled pair of partial differential equations. The first is just Eq. 11 with $M = M(a, t)$, $\Sigma_m = \Sigma_m(a, t)$, while the second is the sum of of the two surface density rates of change:

$$\frac{\partial \Sigma}{\partial t} = \left. \frac{d\Sigma_m}{dt} \right|_{\text{accr}} + \left. \frac{\partial \Sigma_m}{\partial t} \right|_{\text{migr}} \quad (29)$$

We solve this system numerically, for an initially minimum-mass disk identical to the one used to produce Fig. 2. The evolution of M and Σ_m is plotted in Fig. 3. Protoplanet growth now stalls when the planetesimal surface density approaches zero. The results for Σ_m and M in the limit of no planetesimal migration, given by Eqs. 20 and 24, are also shown; the latter approaches a limiting value of M_{iso} . The full solution, however, does not quite reach M_{iso} because of the depletion of planetesimals by gas drag orbital decay. With or without planetesimal migration, by 10 Myrs the largest protoplanet mass is still less than $1 M_{\oplus}$. However, as mentioned in Section 1, the core mass required to form a gas giant planet by nucleated instability is likely $\sim 10 M_{\oplus}$. In our own Solar System, measurements of the mass, radius and gravitational moments of Jupiter and Saturn constrain their present-day solid core masses to be 0 - $10 M_{\oplus}$ and 6 - $17 M_{\oplus}$ respectively (Guillot 1999); it is possible the cores were originally larger, but have since become partially mixed with their envelopes (Guillot 2001). Assuming a protosolar ice/rock ratio, the core masses of Uranus and Neptune are 85-95% of their total masses, that is, 12 - $14 M_{\oplus}$ and 14 - $16 M_{\oplus}$ respectively. This implies that the protoplanetary disk out of which our Solar System formed was well above the minimum mass, and that a minimum-mass disk is in fact unlikely to produce any giant planets at all.

Fig. 4 shows the calculation repeated for a disk which has its solids and gas densities increased by a factor of ten relative to the minimum-mass disk. This yields a solids density of about 25 g/cm^2 around 5 AU, which is a litte below the estimate of Lissauer (1987) for the density needed to accrete Jupiter’s solid core before the dispersal of the nebular gas. In the full numerical solution including planetesimal migration, bodies as large as $10 M_{\oplus}$ form just beyond the snow line in less than 1 Myr. Interior to the snow line, the bodies which have formed by this time are about an order of magnitude smaller. These results show that a strong dependence of protoplanet formation rate on initial solids surface density exists even when the depletion of the disk is accounted for, thus lending support to the theory that the solids density enhancement beyond the snow line facilitates giant planet core formation (Morfill 1985).

In this case, the gas drag-induced orbital decay of planetesimals makes a significant difference in the later stages of accretion. In the migration-less solution (dashed curves), protoplanet masses get above $60 M_{\oplus}$! In the full numerical solution, on the other hand, growth already stalls at a little over $10 M_{\oplus}$ due to the rapid orbital decay of planetesimals

stirred by protoplanets of this size.

Also noteworthy is the fact that very little accretion is predicted to take place in the trans-Saturnian region in 10 Myrs. By this time, a $10\times$ minimum-mass system does not produce even $1 M_{\oplus}$ bodies beyond about 15 AU. The protoplanet mass at the location of Uranus, ~ 20 AU, is only about a tenth of an Earth masses. The simplest description of oligarchic growth, in which the planetesimal surface density is constant (Eq. 14), is a good approximation of the early stages of the process, when protoplanets are small compared to their isolation mass (Eq. 21). From Eq. 14, the protoplanet mass at a given location and time scales as Σ_m^3 . Thus the surface density would have to be higher by at the very least a factor of $(10/0.02)^{1/3} = 8$, i.e. $80\times$ the minimum mass, in order to produce a body of order $10 M_{\oplus}$ at the location of Uranus in 10 Myrs. The minimum-mass protoplanetary disk contains a total mass of about $0.02 M_{\odot}$ within 100 AU; 80 times that is $1.6 M_{\odot}$, far above the typical range of observationally inferred disk masses, ~ 0.01 to $0.2 M_{\odot}$ (eg. Beckwith and Sargent 1996, Chiang et al 2001). Also, such a disk would have a Toomre Q parameter less than one beyond about 20 AU, thus being unstable to collapse outside that radius, and at best marginally stable throughout most of the region inside (eg. Nelson et al 1998).

The apparent inability of much of anything to accrete over 10 Myrs in the trans-Saturnian region presents a definite obstacle to understanding the formation of our Solar System. After all, the $1 - 3 M_{\oplus}$ gas atmospheres of Uranus and Neptune imply that they are composed of protoplanets which, *during* the lifetime of the nebular gas, grew large enough to retain significant atmospheres. In fact, the problem of Uranus and Neptune’s formation timescale is even more severe, as will be discussed in Section 6.

4. The effect of planetesimal size

The efficiency of protoplanet accretion in this model is subject to two competing effects, both of which, for a given nebular gas density, depend on the characteristic planetesimal size. On the one hand, smaller planetesimals experience stronger damping of random velocities, forming a thinner disk and thus increasing the accretion rate. On the other hand, smaller planetesimals are also subject to faster orbital decay, which depletes the planetesimal surface density at a given location in the disk more rapidly. In other words, a smaller planetesimal size means faster accretion, but also an earlier end to accretion. Thus for a finite available time—the lifetime of the nebular gas—there will be an optimal planetesimal radius r_m^{crit} , which produces the largest final protoplanet mass. Using, again, the $10\times$ minimum-mass disk, we compute the protoplanet mass after 10 Myrs as a function of planetesimal size at different stellocentric distances. The result is shown in Fig. 5. The optimal protoplanet

size at 5, 10 and 30 AU is just under 100 km, a few kilometers, and a few tens of meters, respectively (one should be a bit cautious about the last value, which is comparable to the mean free path of gas molecules at 30 AU for our assumed nebula; this puts us at the limit of the validity of the Stokes drag law). Our choice of 10 km planetesimals places us logarithmically near the middle of the optimal range for the Jupiter-Saturn region; at the same time, even if the planetesimal size at 30 AU had happened to be optimal, the largest protoplanet produced there in 10 Myrs would still have been only a few tenths of an Earth mass. Another way to look at the above results is in terms of the planetesimal size spectrum which will exist in real life (recall that we are approximating the planetesimals as a uniform-sized population): Accretion is fastest but least efficient from the small end of the spectrum, and slowest but most efficient from the large end.

5. Validity of the estimate

A number of simplifications underlie this estimate of protoplanet growth rates. To begin with, interactions among planetesimals are neglected altogether in our analysis. This seems reasonable since, by definition, scattering by protoplanets dominates the planetesimal velocity distribution in the oligarchic regime. Also, Kokubo and Ida (2002) showed that the timescale for spreading of the planetesimal disk due to mutual interactions is large compared to the accretion timescale (though the disk *does* spread significantly due to stirring by protoplanets, as will be demonstrated by the numerical simulations in Section 7 below). However, the protoplanets’ dominance of the planetesimal dynamics also means that the relative velocities among planetesimals are large compared to their surface escape velocities. Thus, reprocessing of the planetesimal population through physical collisions can potentially bring about a significant decrease in the characteristic planetesimal size. Inaba and Wetherill (2001) performed statistical simulations in the Jupiter-Saturn region; for their adopted fragmentation model, they found that a substantial fragmentation tail of small bodies formed, resulting in a high loss rate of solids due to gas drag and significantly reduced accretion efficiency relative to the case without fragmentation. If fragmentation was indeed very effective, it would constitute a significant obstacle to the formation of giant protoplanets; it can easily be seen from Fig. 5 that if the majority of the planetesimal mass ends up in, say, bodies with radii of order 100 m, then the largest protoplanets to form will only be a bit over an Earth mass.

Another effect of inter-planetesimal collisions will be to dissipate some of the energy in planetesimal random motions. We can easily estimate the importance of this effect relative to the damping by gas drag. The timescale for the latter is given by Eq. 9. For the former

effect, the lower limit on the timescale is just the time between inter-planetesimal collisions. The collision rate can be estimated as $n(\pi r_m^2)v_{\text{rel}}$, where n is the volume number density of planetesimals, $n \sim \Sigma_m/(mh) \sim \Sigma_m/(mae_m)$, and $v_{\text{rel}} \sim e_m a \Omega$. The collision timescale can thus be written as

$$T_{\text{coll}} \sim \frac{4r_m \rho_m}{3\Sigma_m \Omega}; \quad (30)$$

note that it is independent of random velocity. Setting $T_{\text{coll}} = T_{\text{gas}}^{e_m}$ and solving for e_m , one obtains the very simple expression for the eccentricity at which the two timescales are equal:

$$e_{\text{coll=gas}} \sim \frac{2\Sigma_m}{C_D a \rho_{\text{gas}}}, \quad (31)$$

which is fully determined (within C_D , which we take to be one) by just the gas-to-solids ratio plus the profile of the gas scale height; keeping these fixed, $e_{\text{coll=gas}}$ is unchanged when one scales the disk mass up or down. We plot $e_{\text{coll=gas}}$ for a Hayashi-profile disk in Fig. 31. For $e > e_{\text{coll=gas}}$, the gas drag timescale is shorter. Since the collision timescale has to be the lower limit to the timescale for random velocity damping by collisions, what we have plotted here constitutes the upper limit to the eccentricity at which damping by gas drag comes to dominate over damping by collisions. This limit is of order a few times 10^{-3} , thus from Eq. 10, inter-planetesimal collisions can only dominate early on, when only small bodies have formed and the disk is still dynamically quite cold. It is therefore reasonable to neglect collisional damping while gas is present, though one must still remember that collisions may reduce the characteristic planetesimal size over time.

Perhaps most problematic is the issue of migration due to resonant interaction with the gas disk. Protoplanets embedded in a gas disk launch density waves at their inner and outer Lindblad resonances, and as a result experience a positive and negative torque from the inner and outer parts of the disk, respectively (Goldreich and Tremaine 1980). The outer torque dominates, resulting in a decay of the protoplanet’s orbit, which has been termed Type I migration (Ward 1997). The migration rate increases with protoplanet mass until the protoplanet is large enough to open a gap in the gas disk, and then it is locked into the slower viscous evolution of the disk (Type II migration). However, since protoplanets likely do not form a gap until they reach a mass of $\sim 10 - 100 M_{\oplus}$, and since before that, the migration timescale at 5 AU can be as short as a few times 10^4 years, this poses a problem—not just for this approach to estimating growth times, but for our understanding of the formation of giant planets in general. It has been proposed that fast inward migration could actually speed accretion (Ward 1986); this requires that the protoplanet plough through a pristine, dynamically cold planetesimal disk on its way in. However, given the shorter growth timescales at smaller stellocentric radii, a migrating protoplanet ought to encounter, instead, the dynamically hot remnant of the part of the disk which has already formed protoplanets.

Furthermore, simulations have shown that even in the idealized case, accretion efficiency is low and the disk has to be enhanced by at least a factor of five relative to minimum mass in order to allow a protoplanet starting at 10 AU to reach gap-opening mass before it falls into the star (Tanaka and Ida 1999).

On the other hand, it should be pointed out that the gravitational interaction of a protoplanet with a gas disk is still far from well understood. For one thing, self-consistent simulations of multiple non-gap-opening bodies in a gas disk have, to our knowledge, not yet been performed; it is not clear what happens when a number of bodies launch density waves in close proximity to each other. Conceivably, this could lead to only the inner- and outermost members of a population of protoplanets being strongly coupled to the disk. Also, Papaloizou and Larwood (2000) find that for eccentricities such that the radial excursion is equal to the scale height of the gas disk, the direction of orbital migration actually reverses. Thus, eccentricity-raising interactions among the protoplanets could in principal counteract their orbital decay. However, it is difficult to see how such high protoplanet eccentricities ($h/r \sim 0.07$ at $r=5$ AU) could arise, since Type I-regime torques cause eccentricity to decay on an even shorter timescale than semimajor axis. Furthermore, it has been shown (Tanaka, Takeuchi and Ward 2002) that if the density waves excited by a planet reflect at the outer disk edge, the torque asymmetry can be weakened and a nonmigrating steady state may be attainable. Finally, it is possible that the gap opening mass is smaller than has been thought thus far (eg. Rafikov 2002). In any case, we defer the issue of Type I migration during giant planet accretion to future work. For the present, whenever the protoplanet mass somewhere in the disk approaches an Earth mass, either in our analytic estimates or in the subsequent simulations, one should recall that we are dealing with the limit of no disk torques.

6. Oligarchic growth in the absence of gas

We have established above that collisional damping of random velocities is of little importance in the oligarchic growth regime while the gas is present. However, once the gas is removed, this may no longer be true. The issue of post-gas accretion is of particular interest in the case of our Solar System, since from Section 3, the in situ formation of Uranus and Neptune during the gas lifetime appears to be ruled out. Assuming the problem of the ice giants’ gas content can be otherwise solved, how well can they grow after the gas is gone?

Given the limited knowledge which exists about the behaviour of planetesimals in high-speed collisions—not a problem amenable to direct laboratory study—it is quite uncertain just how effectively these would dissipate energy, and what role fragmentation would play. We therefore look at the two extreme cases: a collisionless planetesimal disk, and a disk in

which the random velocity damping timescale is equal to the collision timescale.

6.1. The collisionless case

Without any damping, an equilibrium planetesimal random velocity no longer exists. It thus becomes necessary to simultaneously solve differential equations for the growth rate and the evolution of the planetesimal random velocity, v_m . Following the approach of Safronov (1969), we estimate the latter as

$$\frac{dv_m^2}{dt} = \frac{v_m^2}{T_{\text{rel}}} \quad (32)$$

with T_{rel} being the gravitational relaxation time (eg. Binney and Tremaine 1987):

$$T_{\text{rel}} \simeq \frac{1}{n_M \pi (2GM/v_m^2)^2 v_m \ln \Lambda}, \quad (33)$$

where n_M is the volume number density of perturbers (protoplanets), and Λ is approximately the ratio of the maximum encounter distance (taken to be the disk scale height) to the minimum non-collisional encounter distance (taken to be the gravitationally enhanced capture radius of the protoplanet); details are given in Stewart and Wetherill (1988). Similar expressions derived for the general velocity evolution of a planetesimal swarm are only valid at low random velocities, otherwise the relative velocities between planetesimals are not properly accounted for (eg. Stewart and Ida 2000). However, for our simple case of one population of bodies on circular orbits stirring another population, taking the relative velocity to be the velocity dispersion of the latter should constitute a reasonable (rough) approximation.

The accretion rate is given by Eq. 6 with $v_{\text{rel}} = v_m$ and $h = v_m/(\sqrt{3}\Omega)$. Eqs. 6 and 32 are integrated, using a surface 10 times that of the minimum-mass model. Since the isolation mass in the giant planet region of such a massive nebula is about an order of magnitude higher than the mass we are trying to attain ($\sim 10 M_{\oplus}$), and since we are interested in the upper limit of accretion efficiency, we take Σ_m to be constant. Protoplanets are taken to be initially Mars-mass ($0.1 M_{\oplus}$, well above the predicted mass at 20 AU at the time of gas dispersal), and the ratio of velocity dispersion to local Keplerian velocity ($= e$) is initially set at 10^{-2} . The accretion rate is set to zero once $\sqrt{v_K^2 + v_m^2}$ is equal to the escape velocity from the primary, $\sqrt{2GM_*/a}$, i.e. $v_m = v_K$. Once random velocities have been raised this high, the density of planetesimals will have been substantially depleted by ejection, and accretion is deemed to have effectively ceased. This is a rather generous estimate of the length of the regime over which accretion operates; it can also be argued (eg. Vityazev and Perchernikova 1991) that the planetesimal disk ought to already be largely depleted when v_m is only $\sim 0.3 - 0.4 v_K$.

Fig. 7 shows the results of the post-gas numerical integration at 10^8 and 10^9 years. Even in 10^9 years, protoplanets at the locations of Uranus (~ 20 AU) and Neptune (~ 30 AU) only grow to $4 M_{\oplus}$ and $2 M_{\oplus}$, respectively. Also plotted is M_{stall} , the mass at which accretion is throttled by the escape of planetesimals. In the Uranus-Neptune region, it is only 4 to $5 M_{\oplus}$. Thus it appears that in the collisionless limit, a $10\times$ minimum-mass disk is unable to oligarchically produce Uranus and Neptune in situ on *any* timescale. It takes a $35\times$ minimum-mass disk to make $M_{\text{stall}} = 10 M_{\oplus}$ at 30 AU. Thirty-five times the minimum mass disk ($\sim 0.02 M_{\odot}$) is about $0.7 M_{\odot}$. This is several times more than the typical range of observed disk masses (~ 0.01 to $0.2 M_{\odot}$; see Section 3). Also, if one supposes that the Solar System grew from such a massive protostellar disk, it becomes difficult to explain why it does not presently contain more mass—especially in the terrestrial region, where it is difficult for material to be ejected.

6.2. The case of perfect collisional damping

Next, we look at what happens when planetesimal random velocities are damped on the timescale of inter-planetesimal collisions. In this case there exists, once again, an equilibrium eccentricity. It is obtained by equating the collision timescale, Eq. 30, to the viscous stirring timescale, Eq. 8. The result is

$$e_m^{\text{eq}} = 1.7 \frac{m^{1/3} \rho_m^{2/3}}{(b \Sigma_m)^{1/4}} \left(\frac{M}{M_{\odot}} \right)^{5/12} \quad (34)$$

If we substitute this into the expression for the protoplanet growth rate, Eq. 7, let Σ_m be constant in time and solve, we get

$$M(t) = \frac{D^2}{4} \left(\frac{2M_0^{1/2}}{D} + t \right)^2 \quad (35)$$

where

$$D^2 = \frac{18.0 b G M_{\odot}^{2/3} \Sigma_m^3}{(\rho_m \rho_M)^{2/3} m^{1/3} a}$$

As mentioned in the previous section, the simplifying assumption of a constant planetesimal surface density is reasonable as long as protoplanet masses are far below M_{lim} . In this case, since the disk is dissipational, the surface density will also decrease due to planetesimal orbital decay. However, since we are interested in the upper limit on protoplanet growth, our approximation will suffice.

Fig. 8 shows the protoplanet masses computed from the above expression, for the same $10\times$ minimum-mass disk as in the previous section. The results for both 10 km and 1 km planetesimals are shown. In 10^8 years, the 10 km case produces neither a Uranus nor a Neptune in situ; the 1 km case does exceed the mass of Uranus at 20 AU but only reaches a few Earth masses at 30 AU. By a billion years, both cases have exceeded the masses of Uranus and Neptune at both 20 and 30 AU. The protoplanet mass is $\propto \Sigma_m^3 r_m^{-1} t^2$ as long as Σ_m has not changed much and M_0 is small; for example, given that something like a Neptune can be grown with $\Sigma_m = 10 \Sigma_m^{\min}$ and $r_m = 10$ km in $t \sim 10^9$ years, one can shorten the timescale to 10^8 years by increasing the surface density to a bit under $50 \Sigma_m^{\min}$, decreasing the planetesimal size to ~ 100 m, or some combination thereof. Thus, it would appear that collisional damping does offer a hope for growing large bodies in the trans-Saturnian region. However, one must keep in mind that the above growth rate estimates are very much upper limits. For comparison, Davis, Farinella and Weidenschilling (1999) report on a statistical multizone simulation in the region from 24 to 50 AU, using an approximately $4\times$ minimum-mass planetesimal disk. Though they model collisional damping, growth already stalls at low masses, and by 4.5 billion years the largest bodies which have accreted are less than $1 M_\oplus$.

6.3. The question of Uranus and Neptune

The actual growth rate after gas dispersal should, at best, lie somewhere between the limiting cases of Sections 6.1 and 6.2; even our lower limit may well be overly optimistic. Thus, it may not be possible to form Uranus- and Neptune-like planets at all in the trans-Saturnian region of a protoplanetary disk, and if it is, the time needed may easily approach the age of the Solar System.

One way to shorten the timescale is to presume a larger disk mass, but as discussed in Section 6.1, one can only go so far before coming into conflict with observational results. The other possibility is to presume that the planetesimal size in the trans-Saturnian region was very small, either primordially or as a result of collisional fragmentation, so that collisional damping was strong. The primordial size cannot be arbitrarily small, since the trans-Saturnian region has to survive millions of years of gas drag without being cleared of planetesimals. Fig. 5 gives an idea of the lower limit, since if planetesimals are of the optimal size r_m^{crit} for accretion in the presence of gas (or smaller), this will leave the region largely cleared of planetesimals by the time the gas disperses. Fig. 5 shows that r_m^{crit} is around 20 m at 30 AU, so during the gas-dominated phase, the characteristic planetesimal size there must have been well above that in order to allow the possibility of significant post-gas ac-

cretion. However, planetesimals could have been collisionally ground down to less than their primordial size subsequent to the dispersal of the gas. We defer a more detailed analysis of the role of planetesimal fragmentation the post-gas oligarchic growth regime—where it may help rather than hinder accretion—to future work.

An alternative way to account for the existence of Uranus and Neptune in the outer Solar System is to lift the requirement that they formed in situ. Zharkov and Kozenko (1990) propose that during the final growth phase of a gas giant, it ejects protoplanets outward which can serve as the starting point for growing the next giant planet. In this way, they suggest that Jupiter triggered the formation of Saturn, which in turn triggered the formation of Uranus and Neptune by launching outward protoplanets of a few Earth masses. Simulations by Ipatov (1991), performed using a Monte Carlo scheme which neglects distant encounters, suggest that this process works if the protoplanets’ eccentricities remain low throughout. However, as demonstrated above, even after such a head start, the growth of the ice giants could stall well before they reach their present masses.

The model of Thommes, Duncan and Levison (1999, 2002) assumes that by the time Jupiter acquired its massive gas envelope, the Jupiter-Saturn region was able to form, in addition to the solid cores of the gas giants, two or more extra bodies of comparable mass. They perform simulations which show that the mass increase of a giant protoplanet becoming a gas giant through runaway gas accretion (presumably Jupiter does this first) causes the remaining protoplanets’ orbits to become unstable. One or more usually undergo close encounters with “Jupiter”, and as a result all of them tend to end up on eccentric, mutually crossing orbits with aphelia in the trans-Saturnian region. Also included in the simulations is a trans-Saturnian planetesimal disk, which serves as a source of dynamical friction for the eccentric protoplanets. As a result, the protoplanets’ eccentricities decrease over time, decoupling them from Jupiter and from each other on a timescale of a few million years. About half of the time, the simulations produce, after 5 - 10 Myrs, a system which is quite similar to our own outer Solar System: Two would-be giant planet cores have ended up on nearly circular, low-inclination orbits with semimajor axes similar to those of Uranus and Neptune, while the third is near the present orbit of Saturn. The timing of the Saturn core’s runaway gas accretion phase is therefore not strongly constrained. Thus, unlike the picture proposed by Zharkov and Kozenko, Uranus and Neptune in this model can be transported outward to their present locations after they have already completed most or all of their growth. Also, scattered protoplanets can be recircularized even after acquiring large eccentricities, by planetesimal disks all the way down to the minimum mass, in contrast to the findings of Ipatov (1991).

This scenario of outward-scattered ice giants appears to fit well with the oligarchic

growth model, provided the protoplanetary disk is of sufficient mass to produce the requisite numbers and sizes of protoplanets. A disk of 10 times the minimum mass contains 130 Earth masses of solids between 5 and 10 AU, well above the combined mass of Uranus and Neptune, plus the upper limits of the heavy element content of Jupiter and Saturn (Guillot 1999). As shown in Section 3, bodies of mass $\sim 10 M_{\oplus}$ are predicted to form in less than a million years. A spacing of $\sim 10 r_{\text{H}}$ allows about four such bodies to fit in the Jupiter-Saturn region. However, the question of how readily this many objects can be produced in the time available—while both gas and planetesimals are still present—must ultimately be addressed with numerical simulations.

7. Numerical simulations

A simple semi-analytic estimate for protoplanet mass as a function of time throughout a protoplanetary disk is a potentially powerful tool, since it offers the possibility of characterizing accretional evolution over time and distance scales which are as yet beyond the reach of numerical simulation. Nevertheless, to assess the validity of such an estimate, comparisons to simulations must be made. The limits of computing capacity restrict the domains of full N-body simulations to relatively narrow annuli within a protoplanetary disk. In the simulations presented below, we are able to simulate larger regions of the disk by making use of simplifications which speed computation but preserve enough of the relevant physics to make the results meaningful.

7.1. Method

The simulations are performed with a variant of SyMBA, a symplectic integrator which makes use of an adaptive timestep to resolve close encounters among bodies (Duncan, Levison and Lee 1998). This version also models the aerodynamic drag force on planetesimals due to a gas disk. The gas disk is modeled with a three-dimensional density profile of the form given by Eqs. 18 and 19, and the parameter η is calculated from Eq. 26.

In the vertical direction, the reference Keplerian velocity for the gas disk changes, since it is the horizontal component of the Solar gravity which provides the central force:

$$v_{\text{K}}^2(a, z) = \frac{GM_{\odot}}{a} (a/\sqrt{a^2 + z^2})^3 \quad (36)$$

Stokes drag is applied to planetesimals:

$$\dot{\mathbf{v}} = -K v_{\text{rel}} \mathbf{v}_{\text{rel}}, \quad (37)$$

where v_{rel} is the velocity of a planetesimal relative to the gas disk. The drag parameter K is

$$K = \frac{3\rho_{\text{gas}}C_{\text{D}}}{8\rho_m r_m} \quad (38)$$

and we again adopt $C_{\text{D}} = 1$.

A number of simplifications are made to render feasible the task of simulating proto-planet growth over a radial range of up to tens of AU for millions of years. First, to prevent the computational expense from being prohibitive, the planetesimal disks are built up of bodies much larger than a realistic characteristic planetesimal (~ 1 to 100 km, corresponding to 10^{-12} to $10^{-6} M_{\oplus}$). We adopt planetesimal masses of 0.01 to $0.05 M_{\oplus}$. However, for the purpose of calculating the gas drag, the actual planetesimal size is not used. Using the approach of Beauge, Aarseth and Ferraz-Mello (1994) we instead assume a more physically realistic size of 1 or 10 km ($\sim 10^{-12}$ or $10^{-9} M_{\oplus}$) and apply the drag accordingly. Thus, each small body in the simulation can be regarded as a “super-planetesimal” representing the averaged orbits of a large number of real planetesimals.

With such large planetesimals, one must ensure that the protoplanets are sufficiently larger, otherwise they will not experience effective dynamical friction. From test runs, we determined that an order of magnitude difference between the populations is enough to keep the protoplanets’ eccentricities and inclinations reasonably low. Also, using super-planetesimals increases the planetesimal accretion rate of a protoplanet, since the physical interaction radius is the sum of both bodies’ radii, and since in the realistic case the planetesimal radius is negligibly small compared to that of the protoplanet. A factor of ten mass difference gives a factor of about two difference in radii, and thus a growth rate $\propto (r_M + r_m)^2$ which is initially too high by a factor of roughly two. The fractional error decreases as the protoplanets grow and widen the protoplanet-planetesimal size gap.

The large starting mass of the protoplanets constitutes an unrealistic initial condition; for example, from the semianalytic estimate, protoplanet masses at 10 AU need several million years to reach $0.1 M_{\oplus}$ if they are initially $\ll 0.1 M_{\oplus}$ (Fig. 4). Thus the simulations give the protoplanets a significant head start. Again, this leads to a smaller fractional error in protoplanet growth rates for larger protoplanets, and since the timescale to reach the final mass is dominated by the time spent in the later phases, the oversized protoplanets are a reasonable initial condition.

Finally, just as in the semi-analytic estimate, planetesimal-planetesimal interactions—both gravitational and collisional—are neglected. The planetesimals are treated as a non-self-interacting population by the integrator, though each one fully interacts with all protoplanets, thus making these “N+N’-body” simulations in which the computation time scales quadratically with N (the number of protoplanets) but only linearly with N’ (the number

of planetesimals). Another benefit of neglecting gravitational interactions among planetesimals is that it prevents self-stirring of the planetesimal population which, given their large masses and lack of softening—at present SyMBA does not support softened potentials due to the way close encounters are handled—would result in unrealistically high eccentricity and inclination growth rates. (Partially) inelastic collisions between planetesimals, on the other hand, would act to reduce their random velocities, but as shown in Section 5, this effect is negligible compared to damping by gas drag. In the simulations, collisions between protoplanets and planetesimals, or between two protoplanets, are treated as perfectly inelastic; that is, the two participating bodies are always merged. Work done on the role of fragmentation in late-stage planetary formation (Alexander and Agnor 1998) suggests that this is a reasonable assumption.

7.2. Simulation results

7.2.1. Run A

The first simulation is performed in the vicinity of the snow line (2.7 AU) in the Hayashi disk. The gas and solids surface densities are increased everywhere by a factor of five relative to the minimum mass model. Equal-mass, $0.01 M_{\oplus}$ planetesimals are initially distributed between 1.5 and 5 AU. Planetesimals initially have a Rayleigh distribution in eccentricities and inclinations, with RMS values of 0.01 and $0.005 (= 0.29^{\circ})$ respectively, somewhat lower than what is given by Eq. 10 ($e_m \simeq 0.03 \simeq 2i_m$). However, since the timescale to reach e_m^{eq} once the simulation commences is short compared to that for accretion (see Eq. 13), unrealistically low initial planetesimal random velocities have little effect on the outcome of the simulation. The protoplanets are given equal masses of $0.1 M_{\oplus}$, and are distributed over the same range in semimajor axis, with successive bodies spaced about $10 r_H$ apart. Planetesimal densities are set at 3 g/cm^3 . The density of ice-enhanced material beyond the snow line would have been lower—perhaps only half of this—but since growth rates are not a strong function of the body densities, a single density is used for the planetesimals. Protoplanets outside the snow line are given an initial density of 1.5 g/cm^2 , but because SyMBA averages densities when bodies merge, their densities also approach 3 g/cm^3 as they accrete planetesimals. Gas drag commensurate with a size of 10 km is applied to the planetesimals. The fractional difference η between Keplerian velocity and the gas orbital velocity is of order 10^{-3} .

The total simulation time is 1 Myr. Snapshots of the protoplanet masses and semimajor axes at .05, .1, .5 and 1 Myrs are shown in Fig. 9. Also plotted are the estimates of protoplanet mass, obtained from solving Eqs. 11 and 29 with an initial mass of $0.1 M_{\oplus}$,

and with the physical protoplanet cross-section increased to take into account the large planetesimal radii ($r_M \rightarrow r_M + r_m$). Protoplanet growth stalls earlier than predicted, with little change in protoplanet masses between 0.5 and 1 Myrs; there is primarily just an overall spreading of protoplanet orbits over that time. Since the planetesimals spread with the protoplanets, the expansion of the protoplanet system beyond the original radial extent of the planetesimal disk acts to lower the planetesimal surface density, and thus slow growth, relative to the analytic description. The largest protoplanet at 1 Myr has a mass of $2 M_\oplus$; the largest model-predicted mass at this time is around $6 M_\oplus$. The assumption of a $10 r_H$ orbital spacing is roughly borne out by the largest protoplanets.

A jump in protoplanet mass does seem to exist at the snow line for a while, particularly at 0.1 Myrs. At later times this jump becomes washed out. But this is to be expected, since both protoplanets and planetesimals diffuse in semimajor axis as they gravitationally interact with each other, and since the simulation does not “enforce” the snow line once it starts running. In other words, sublimation/freezing of ice/water crossing the boundary is not modeled.

Fig. 10 shows the state of the simulation at 1 Myr in more detail, including planetesimal eccentricities and inclinations. The eccentricities and inclinations are comparable to the predicted values beyond 3 AU. However, inside 3 AU, only two protoplanets remain and these have opened a shared gap, thus halting accretion. As a result, the planetesimal random velocities here are significantly lower than predicted. The effect of migration of planetesimals due to gas drag can be clearly seen here. Over time, more and more are deposited interior to (most of) the protoplanets, forming a broadening, dense, dynamically cold ring. This happens because less eccentric planetesimal orbits decay less rapidly (see Eq. 25), so that once planetesimals are out of range of strong gravitational stirring by the protoplanets, their radial motion slows and they pile up. Orbital repulsion between the protoplanets and these massive rings—at 10^6 years, there are about $14 M_\oplus$ in planetesimals between 2.5 and 3 AU, and about $16 M_\oplus$ interior to 2 AU—further promotes the segregation between the planetesimal and protoplanet populations.

The formation of dynamically cold planetesimal rings like those seen in this and subsequent runs is a simulation artifact, unlikely to occur in a real system. In actuality these planetesimals would have been further scattered by protoplanets already formed at smaller stellocentric distances. Alternatively, in cases where a high density of planetesimals really did accumulate in a region largely devoid of gravitational stirring by protoplanets, they would simply revert temporarily to runaway growth and spawn new protoplanets in their midst. Therefore, the end state of Run A is almost certainly a poor representation of reality interior to 3 AU. In particular, the dense planetesimal ring between 2.5 and 3 AU would

have produced much more protoplanet growth, and thus the analytic estimate of protoplanet mass would have been better reproduced in that region than it is in the simulation. At the same time, as long as a region of the disk is, for whatever reason, predominantly stirred by only one or a few protoplanets, the opening of a gap like that in Run A (and subsequent runs) is a likely outcome (Rafikov 2001).

7.2.2. Run B

The next simulation we present uses a planetesimal disk with an initial surface density

$$\Sigma_m^B = 250(a/1 \text{ AU})^{-2} \text{g/cm}^2 = 10(a/5 \text{ AU})^{-2} \text{g/cm}^2, \quad (39)$$

extending from 5 to 15 AU. This is suggested by Pollack et al (1996) as the optimum surface density for the accretion of the giant planets. It is 3.7 times the minimum-mass surface density at 5 AU. The corresponding gas nebula is therefore given a midplane volume density of 3.7 times its value at 5 AU and a density profile $\propto a^{-2-5/4} = a^{-13/4}$, under the assumption that the gas scale height also has the profile of Eq. 19. The gas volume density is thus

$$\rho_{\text{gas}}^B = 1.15 \times 10^{-8} (a/1 \text{ AU})^{-13/4} \text{g/cm}^3 \quad (40)$$

The planetesimal disk consists of equal mass bodies of $0.02 M_{\oplus}$. In this disk, protoplanets of initial mass $0.2 M_{\oplus}$ are placed at intervals of approximately ten Hill radii. For the application of gas drag, the planetesimals are, again, assumed to have a size of 10 km.

The length of the run is 10 Myrs. Snapshots of the protoplanet masses and semimajor axes at 0.5, 1, 5 and 10 Myrs are shown in Fig. 11. Fig. 12 gives the state of the run at 10 Myrs in more detail, showing also the eccentricities and inclinations of the protoplanets and planetesimals. The largest protoplanet which has formed by this time has a mass of $2 M_{\oplus}$. The location of the growth front matches that predicted by the model quite well throughout the run. Agreement with the theoretical protoplanet masses beyond 5 AU is likewise quite good initially, however the masses reached after the growth front has largely swept past, inside 6 - 10 AU at 1 - 10 Myrs, are smaller than the predicted final masses by a factor of several. This appears to be at least partly an edge effect: Under the action of stirring by protoplanets, the planetesimal disk spreads—this is superimposed on the net inward migration of planetesimals—which further lowers the disk surface density, particularly near the edges. Since protoplanets grow fastest and orbital times are shortest at the inner edge, the surface density there is affected most strongly. Fig. 13 shows that the surface density near the inner edge of the protoplanet population, around 5 AU, is indeed lower than the analytic estimate after about a million years. As time goes on, this underdense region moves

outward; by 10 Myrs, it reaches all the way out to about 11 AU. In addition, Fig. 12 shows that, similar to the case of Run A, the innermost protoplanet at 10 Myrs has cut short its growth by forming a gap in the planetesimal disk.

Fig. 14 shows the evolution of protoplanet semimajor axes in detail, including their merger history. A total of five mergers among protoplanets take place, reducing their number from the original 16 to 11; no protoplanets are lost to ejection, or otherwise leave simulation domain. In this run, as in the others, mergers among protoplanets only play a secondary role in the accretion process; sweep-up of planetesimals is the primary growth mode, therefore the oligarchic growth model provides a reasonable fit. Also apparent in Fig. 14 is that significant reordering of protoplanet orbits takes place over the course of the run.

7.2.3. Run C

We repeat the above simulation, but with the drag force on the planetesimals increased to what 1 km objects would experience. Snapshots of the run are shown in Fig. 15, and the endstate, at 10 Myrs, is shown in Fig. 16. In keeping with what the model predicts, the growth front moves outward more rapidly than in Run B. The largest protoplanet at 10 Myrs is just under $2 M_{\oplus}$, very similar to Run B, although the predicted largest protoplanet mass is only about half that of Run B. The theoretically predicted discrepancy comes about because smaller planetesimals ought to bring about faster growth, at the expense of a smaller final mass, as discussed in Section 4. However, the analytic protoplanet masses in Run B are only larger than those of Run C inside about 8 AU at 10 Myrs. In both runs, the growth of protoplanets in the inner region is stunted by simulation edge effects, as described in Section 7.2.2 above.

7.2.4. Run D

Lastly, we show the result of a simulation performed with a more massive initial protoplanetary disk. The solids surface density is chosen as

$$\Sigma_m^D = 20(a/5 AU)^{-3/2} \text{g/cm}^3, \quad (41)$$

which is about 7.5 times that of the minimum-mass nebula. The gas surface density is increased above minimum mass by the same factor, and the half-thickness is assumed to be, again, given by Eq. 19. The total mass in planetesimals is about 2.7 times as large as in Run B, so to keep the number of bodies reasonably low, more massive bodies are used in

Run D. The planetesimal mass is changed to $0.05 M_{\oplus}$, and the protoplanet initial mass to $0.5 M_{\oplus}$.

The length of this run is 5 Myrs; snapshots at 0.1, 0.5, 1 and 5 Myrs are shown in Fig. 17, and the endstate is shown in more detail in Fig. 18. The run produces a largest body of $5 M_{\oplus}$ just inside 9 AU by 5 Myrs, and a total of four bodies that are more massive than $3 M_{\oplus}$. The initial growth rate is again faster than predicted, but the masses produced once the wave of growth has swept past, inside 9 AU at 5 Myrs, are lower than the theoretical value by a factor of several. Fig. 18 shows only a small number of planetesimals remaining among the protoplanets interior to the growth front, confirming that accretion there has essentially concluded.

8. Conclusions

Runaway growth allows very short formation times, but only in the early stages of planetesimal accretion; there is a transition to the self-limiting oligarchic growth mode when the largest bodies are still orders of magnitude below an Earth mass. The timescale of oligarchic growth thus dominates over that of runaway growth, and we use the former alone to obtain a global picture of planet formation throughout a protoplanetary disk. In the terrestrial region, accretion efficiency is high, and oligarchic growth alone is not required to form final bodies of terrestrial-planet masses. Simulations show that a late stage of impacts among protoplanets of up to perhaps Mars mass is readily able to produce a final system with planet masses and spacings similar to the present-day inner Solar System (eg. Chambers and Wetherill 1998). A significant planetesimal population is not necessary to facilitate late-stage accretion, though it may be needed to reproduce (via dynamical friction) the low eccentricities of the terrestrial planets.

In the giant planet region, however, lower accretion efficiency and the necessity of forming large bodies before the removal of the nebular gas (after $\lesssim 10$ Myrs) mean that direct oligarchic growth likely has to be relied on to account for most of the accretion. In our semi-analytic model, the outward-sweeping front of oligarchic growth produces $10 M_{\oplus}$ bodies in a protoplanetary disk with ten times the mass of the Hayashi (1981) minimum-mass model in less than a million years. These first appear near the snow line, where the surface density enhancement gives accretion a head start and increases the maximum attainable masses. Thus, the snow line may indeed play a role in triggering the formation of giant planets, as has been previously suggested (Morfill 1985).

The numerical simulations performed here agree reasonably well with the model insofar

as the timing of the initial oligarchic growth front is concerned. However, accretion stalls earlier than predicted, and the largest final masses produced typically fall short of the theoretical values by factors of several. This can be attributed in part to a simulation edge effect, namely, the spreading of the simulated planetesimal disk beyond its initial radial extent, which causes the disk surface density to decrease faster than the model (which does not incorporate this effect) predicts; the effect is strongest at the inner edge of the disk. Another edge effect is that the innermost few protoplanets act more like isolated bodies in a planetesimal disk, because there are fewer neighbouring stirred regions which overlap theirs. Consequently, they tend to open a gap in the planetesimals, thus putting a premature end to their growth (Rafikov 2001). Gap formation about the innermost protoplanets is evident in Figs. 10, 12 and 16. In order to make the inner edge less artificial, future simulations ought to include additional larger protoplanets interior to the planetesimal disk, to play the role of the “endproducts” in the region where oligarchic growth has already reached completion. However, given that protoplanets interior to the snow line are expected to reach significantly smaller final masses, edge effects like those in our simulations may not be completely unrealistic. In any case, it appears that the semi-analytic estimate we have developed here for the oligarchic growth endproduct masses is an upper limit.

Overall, then, it is still somewhat of a challenge to understand how (potential) gas giant cores can form in a protoplanetary disk. The formation of an extended gas atmosphere on larger protoplanets, not modeled here, will certainly help in sweeping up planetesimals. It may simply be that the protoplanetary disks which produce giant planet-bearing systems really are quite massive, perhaps in excess of ten times the minimum mass. However, one can only push the disk mass so far before one comes up against observational limits. Stevenson and Lunine (1988) develop a model in which diffusive redistribution of water vapor from the inner part of the nebula leads to a large local density enhancement near the snow line, so that the jump in solids density there has an additional spike superimposed on it. Another possible scenario is that runaway gas accretion already takes place at smaller core masses, perhaps as little as $1 M_{\oplus}$. This would be facilitated by low grain opacities in the accreting atmosphere (eg. Inaba and Wetherill 2001). Yet another possibility is that the window of opportunity for gas giant formation is larger than normally assumed. Kokubo and Ida (2002) adopt 10^8 rather than 10^7 years as the gas lifetime, pointing out that the timescale for the *complete* dispersal of gas may approach this larger value (Thi et al 2001). However, as the gas density drops, so will the planetesimal accretion rate. Also, it is unclear how much the gas nebula can be depleted before core accretion stops being viable.

In 10 Myrs, the (optimistic) predicted growth front only produces $10 M_{\oplus}$ bodies interior to about 10 AU, even in very massive protoplanetary disks. Thus in the case of our Solar System, although the solid cores of Jupiter and Saturn can be more or less accounted for, it

seems that Uranus and Neptune are out of luck as far as in situ formation during the lifetime of (most of) the gas is concerned. Accounting for the ice giants’ gas content is a problem, since the protoplanets which are predicted to have formed in the trans-Saturnian region by the time the gas disperses are too small to have acquired appreciable atmospheres. The most fundamental difficulty, however, is that of the post-gas growth timescales. If random velocities in the planetesimal disk are not damped at all, then the formation of Uranus- and Neptune-mass planets is not possible on *any* timescale. If collisions among planetesimals are an effective dissipational mechanism, then such planets could conceivably form, though it could well take of order a billion years, during which time the planetesimal disk has to maintain a sufficiently high optical depth to keep the collisions going.

A model in which the ice giants shared the same birthplace as Jupiter and Saturn, only to be scattered outward when Jupiter accreted its massive gas envelope, provides an alternative (Thommes, Duncan and Levison 1999, 2002). Of course, this scenario is predicated on the ability to form multiple $\gtrsim 10 M_{\oplus}$ bodies in the Jupiter-Saturn zone, notwithstanding the above difficulties, while at the same time leaving some of them without massive gas envelopes at the time when the nebular gas disappears. The simulations performed here provide some support for this scenario, in the sense that they show several comparable-mass largest protoplanets occupying the gas giant region after several million years of evolution. Run D, with the largest initial disk mass, looks the most promising. However, the protoplanets produced still fall significantly short of Uranus and Neptune’s core masses. Run D’s protoplanet masses at 10 Myrs would need to be scaled up by a factor of about three; then the largest protoplanets would comprise a system not dissimilar to the initial conditions used in Thommes, Duncan and Levison (1999, 2002)

Orbital evolution through disk tides (eg. Ward 1997) is not considered in this analysis. Fast Type I inward migration, predicted to be strongest for bodies with masses of order 10 - 100 M_{\oplus} , constitutes a major potential problem for any model of giant planet formation, except ones which invoke direct, unnucleated collapse from a gas disk instability (eg. Boss 1998). However, at present it is still quite uncertain just how serious this problem is. For instance, it has been shown that the nature of the migration depends sensitively on the assumed disk boundary conditions (Tanaka, Takeuchi and Ward 2002). Also, Type I migration may be halted at a smaller mass than is commonly assumed (eg. Rafikov 2002).

In the limit of no Type I migration, the investigation presented here suggests the following overall picture of the post-runaway planet formation process: During the first ten million years or less, while the nebular gas is still present, a relatively rapid front of oligarchic growth sweeps outward through the disk. By the time the gas disperses, however, this wave has only reached what corresponds to the Jupiter-Saturn region; very little accre-

tion takes place during this time in the trans-Saturnian region, thus the planetary system is initially quite compact, with a Kuiper belt starting at ~ 10 AU. Bodies large enough to be potential gas giant cores form only in an annulus encompassing roughly the outer half of the (proto-) planetary system's radial extent. Once the gas disappears, the outward-expanding wave of growth becomes far slower and the subsequent formation of giant planets (of necessity gas-poor ice giants like Uranus and Neptune) becomes difficult, perhaps impossible. However, if gas giants are able to form before the removal of the gas, a likely by-product will be the scattering of any remaining giant protoplanets that missed out on acquiring a massive gas envelope. This could ultimately produce an outer planetary system with widely-spaced, circular giant planet orbits like those of the present-day Solar System, while requiring little or no accretion to take place after the gas is gone.

Acknowledgements: This work is supported by the Center for Integrative Planetary Science (EWT), NASA's *Origins of Solar Systems* (EWT, HFL), *Planetary Geology & Geophysics* and *Exobiology* (HFL) programs, and by Canada's National Science and Engineering Research Council (MJD). We would like to thank the referees, Satoshi Inaba and Eiichiro Kokubo, for valuable suggestions which helped us to improve the manuscript. Also, we would like to thank Glen Stewart and Andrew Youdin for helpful discussions.

REFERENCES

- Adachi, I., C. Hayashi and K. Nakazawa 1976. The gas drag effect on the elliptic motion of a solid body in the primordial solar nebula. *Progress of Theoretical Physics* **56**, No. 6, 1756-1771.
- Alexander, S. G. and C. B. Agnor 1998. N-Body Simulations of Late Stage Planetary Formation with a Simple Fragmentation Model. *Icarus* **132**, 113-124
- Beauge, C., S. J. Aarseth, and S. Ferraz-Mello 1994. Resonance Capture and the Formation of the Outer Planets. *MNRAS* **270**, 21.
- Beckwith, S. V. W. and A. I. Sargent 1996. Circumstellar disks and the search for neighbouring planetary systems.. *Nature* **383**, 139-144
- Binney, J. and S. Tremaine 1987. *Galactic dynamics*. Princeton, NJ, Princeton University Press, 1987, 747 p. .
- Boss, A. P. 1995. Thermal profiles in protoplanetary disks. *Abstracts of the Lunar and Planetary Science Conference* **25**, p. 151

- Boss, A. P. 1998. Evolution of the solar nebula. IV. Giant gaseous protoplanet formation. *ApJ* **503**, 923-937.
- Chambers, J. E. and G. W. Wetherill 1998. Making the terrestrial planets: N-body integrations of planetary embryos in three dimensions. *Icarus* **136**, 304-327.
- handrasekhar, S. 1949. *Principles of Stellar Dynamics*, Yale Univ. Press, New Haven, CT.
- Charnoz, S. and A. Brahic 2001. Long-term collisional evolution of a dissipative particle disc perturbed by a giant-planet embryo. *A&A* **375**, L31-L34
- Chiang, E. I., M. K. Joung, M. J. Creech-Eakman, C. Qi, J. E. Kessler, G. A. Blake, and E. F. van Dishoeck 2001. Spectral Energy Distributions of Passive T Tauri and Herbig Ae Disks: Grain Mineralogy, Parameter Dependences, and Comparison with Infrared Space Observatory LWS Observations. *ApJ* **547**, 1077-1089
- Davis, D. R., P. Farinella, and S. J. Weidenschilling 1999. Accretion of a Massive Edgeworth-Kuiper Belt. Lunar and Planetary Institute Conference Abstracts 30, 1883.
- Duncan, M. J., H. F. Levison, and M. H. Lee 1998. A Multiple Time Step Symplectic Algorithm for Integrating Close Encounters. *AJ* **116**, 2067-2077.
- Goldreich, P. and S. Tremaine 1980. Disk-satellite interactions. *ApJ* **241**, 425-441.
- Greenzweig, Y. and J. J. Lissauer 1992. Accretion rates of protoplanets. II - Gaussian distributions of planetesimal velocities. *Icarus* **100**, 440-463.
- Guillot, T. 2001. Mixing the Cores and Envelopes of Giant Planets: Consequences for Formation Models. AAS/Division for Planetary Sciences Meeting 33, .
- Guillot, T. 1999. Interiors of giant planets inside and outside the Solar System. *Science* **286**, 72-77.
- Hayashi, C. 1981. Structure of the solar nebular, growth and decay of magnetic fields and effects of magnetic and turbulent viscosities on the nebula. *Prog. Theor. Phys. Suppl.* **70**, 35-53.
- Ida, S. and Nakazawa, K. 1989. Collisional probability of planetesimals revolving in the solar gravitational field. III. *Astron. Astrophys.* **224**, 303-315.
- Ida, S. 1990. Stirring and dynamical friction rates of planetesimals in the solar gravitational field. *Icarus* **88**, 129-145.

- Ida, S. and J. Makino 1993. Scattering of planetesimals by a protoplanet: Slowing down of runaway growth. *Icarus* **106**, 210-227.
- Inaba, S. and G. W. Wetherill 2001. Formation of Jupiter: Core Accretion Model with Fragmentation. Lunar and Planetary Institute Conference Abstracts 32, 1384.
- Ipatov, S. I. 1991. Evolution of Initially Highly Eccentric Orbits of the Growing Nuclei of the Giant Planets. Soviet Astronomy Letters 17, 113.
- Kokubo, E. and S. Ida 1996. On runaway growth of planetesimals. *Icarus* **123**, 180-191.
- Kokubo, E. and S. Ida 1998. Oligarchic growth of protoplanets. *Icarus* **131**, 171-178.
- Kokubo, E. and S. Ida 2000. Formation of protoplanets from planetesimals in the solar nebula. *Icarus* **143**, 15-27.
- Kokubo, E. and S. Ida 2002. Formation of protoplanet systems and diversity of planetary systems. Preprint, submitted to ApJ
- Levison, H. F. and G. R. Stewart 2001. Remarks on Modeling the Formation of Uranus and Neptune. *Icarus* 153, 224-228
- Lissauer, J. J. 1987. Timescales for planetary accretion and the structure of the protoplanetary disk. *Icarus* **69**, 249-265
- Mizuno, H., K. Nakazawa, and C. Hayashi 1978. Instability of a gaseous envelope surrounding a planetary core and formation of giant planets. *Progress of Theoretical Physics* 60, 699-710
- Morfil, G. E. 1985. Physics and chemistry in the primitive solar nebula. *Birth and Infancy of Stars* (R. Lucas, A. Omant, and R. Stora, Eds.) 693-792. Elsevier, Amsterdam.
- Nelson, A. F., W. Benz, F. C. Adams, and D. Arnett 1998. Dynamics of Circumstellar Disks. *ApJ* 502, 342
- Papaloizou, J.C.B. and J. D. Larwood 2000. On the orbital evolution and growth of protoplanets embedded in a gaseous disk. *MNRAS* **315**, 823-833.
- Pollack, J. B. et al. 1996. Formation of the giant planets by concurrent accretion of solids and gas. *Icarus* **124**, 62-85.
- Rafikov, R. R. 2001. Termination of Planetary Accretion Due to Gap Formation. *AJ* 122, 2713-2722

- Rafikov, R. R. 2002. Planet Migration and Gap Formation by Tidally Induced Shocks. *ApJ* 572, 566-579.
- Safronov, V. S. 1969 *Evolution of the Protoplanetary Cloud and Formation of the Earth and Planets*. Moscow:Nauka. Engl. transl. NASA TTF-677, 1972.
- Sasselov, D. D. and M. Lecar 2000. On the snow line in dusty protoplanetary disks. *Astrophys.J* **528**, 995-998
- Stewart, G. R. and G. W. Wetherill 1988. Evolution of planetesimal velocities. *Icarus* 74, 542-553.
- Stewart, G. R. and S. Ida 2000. Velocity Evolution of Planetesimals: Unified Analytical Formulas and Comparisons with N-Body Simulations. *Icarus* 143, 28-44.
- Strom, S. E., S. Edwards, and M. F. Skrutskie 1990. Evolutionary Time-Scales for Circumstellar Disks Associated with Solar-Type Pre-Main Sequence Stars. AIP Conf. Proc. 207: Astrophysics from the Moon 71.
- Tanaka, H. and S. Ida 1997. Distribution of Planetesimals around a Protoplanet in the Nebula Gas. *Icarus* 125, 302-316.
- Tanaka, H. and S. Ida 1999. Growth of a Migrating Protoplanet. *Icarus* 139, 350-366
- Tanaka, H., T. Takeuchi, and W. R. Ward 2002. Three-Dimensional Interaction between a Planet and an Isothermal Gaseous Disk. I. Corotation and Lindblad Torques and Planet Migration. *ApJ* 565, 1257-1274.
- Thi, W. F., G. A. Blake, E. F. van Dishoeck, G. J. van Zadelhoff, J. M. M. Horn, E. E. Becklin, V. Mannings, A. I. Sargent, M. E. van den Ancker, and A. Natta 2001. Substantial reservoirs of molecular hydrogen in the debris disks around young stars. *Nature* 409, 60-63.
- Thommes, E. W., M. J. Duncan and H. F. Levison 1999. The formation of Uranus and Neptune in the Jupiter-Saturn region of the Solar System. *Nature* **402**, 635-638.
- Thommes, E. W., M. J. Duncan and H. F. Levison 2002. The formation of Uranus and Neptune among Jupiter and Saturn. *AJ* **123**, 2862-2883.
- Vityazev, A. V. and G. V. Perchernikova 1991. Late stages of accumulation and early evolution of the planets. *Planetary Sciences: American and Soviet Research* 143-162.

- Ward, W. R. 1986. Density waves in the solar nebula - Differential Lindblad torque. *Icarus* **67**, 164-180
- Ward, W. R. 1997. Protoplanet migration by nebula tides. *Icarus* **126**, 261-281.
- Weidenschilling, S. J. 1998. Growing Jupiter the Hard Way. AAS/Division for Planetary Sciences Meeting 30, 1050.
- Wetherill, G. W. Formation of the terrestrial planets. *Annu. Rev. Astron. Astrophys.* **18**, 77-113.
- Wetherill, G. W. and G. R. Stewart 1989. Accumulation of a swarm of small planetesimals. *Icarus* **77**, 330-357.
- Zharkov, V. N. and A. V. Kozenko 1990. On the Role of Jupiter in the Formation of the Giant Planets. *Soviet Astronomy Letters* 16, 73.

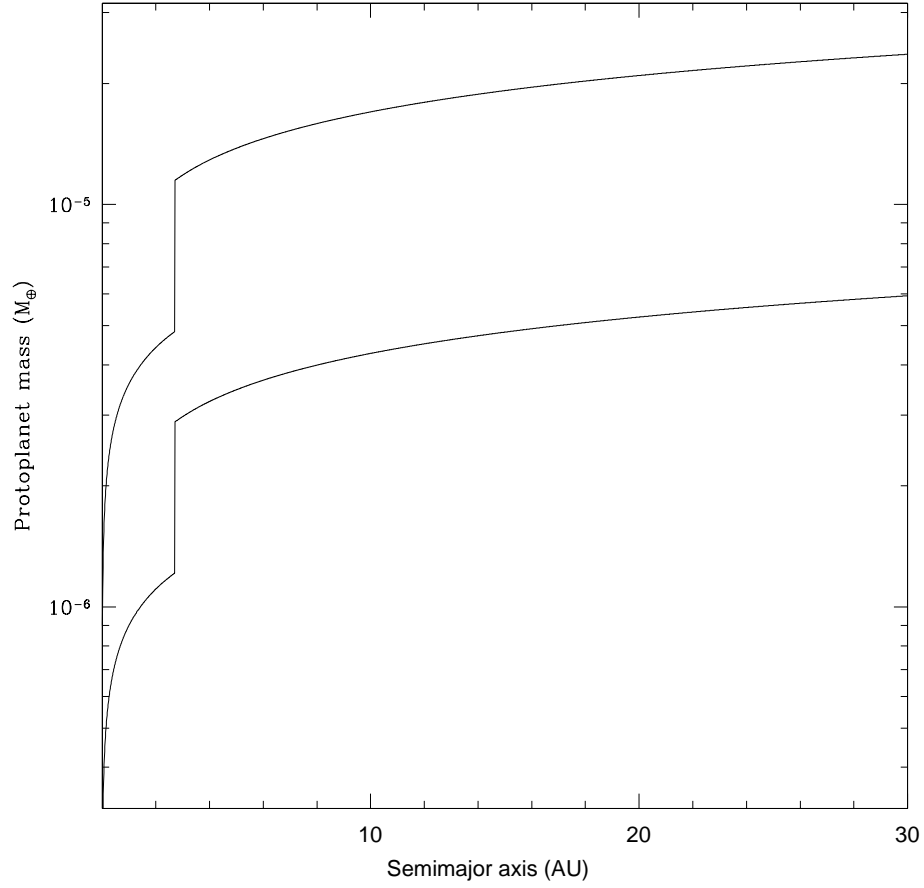


Fig. 1.— Threshold protoplanet mass for crossover from runaway to oligarchic growth in a minimum-mass (lower curve) and $10\times$ minimum-mass (upper curve) nebula, as obtained from Eq. 5. A uniform planetesimal size of 10 km is assumed.

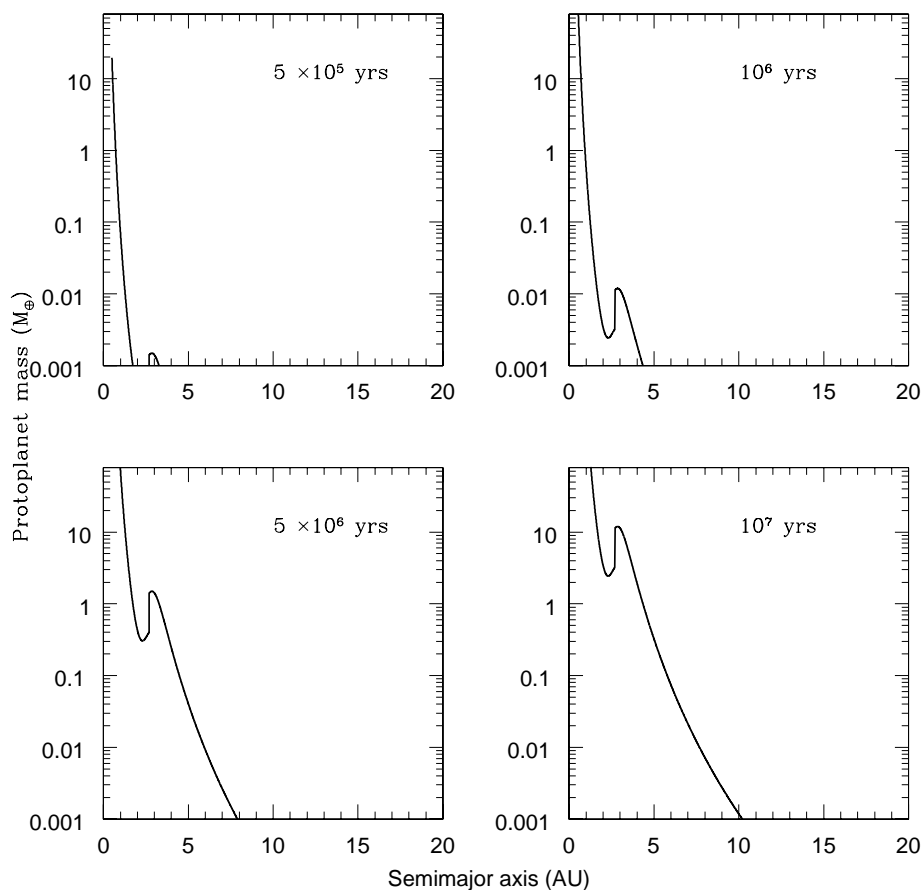


Fig. 2.— The protoplanet mass function for a minimum-mass nebula at 0.5, 1, 5 and 10 Myrs. The curves are computed using Eq. 14, which assumes a planetesimal surface density that is constant over time, so that the protoplanet mass (unphysically) increases without bound. M_0 is taken to be zero; as long as the initial mass is well below the mass range of interest, it has negligible effect on the solution.

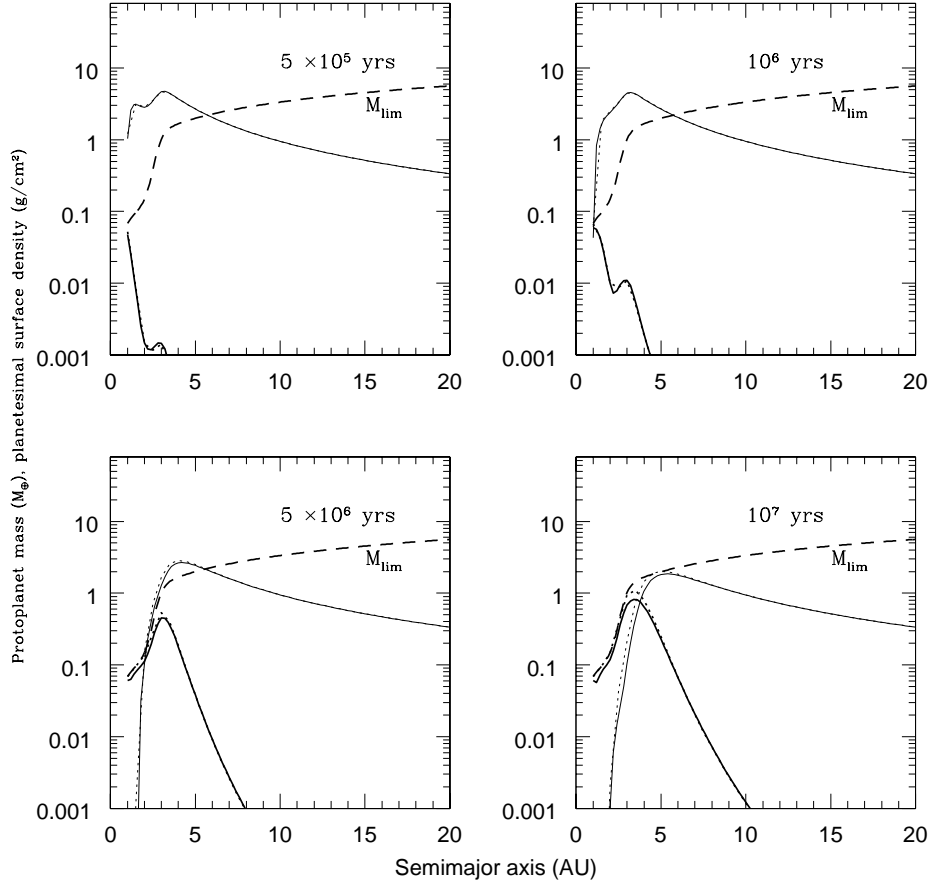


Fig. 3.— Protoplanet mass (thick curves) and planetesimal surface density (thin curves) versus heliocentric distance for a minimum-mass gas nebula (Eq. 17) and an initially minimum-mass planetesimal disk with a smoothed-out snow line discontinuity (Eq. 16) after 0.5 to 10 Myrs of evolution. The solution obtained from numerically integrating the coupled system of Eqs. 11 and 29 is shown as solid curves, while the analytic result when migration of planetesimals is neglected, given by Eqs. 20 and 24, is shown as dotted curves. The migrationless solution approaches the isolation mass M_{lim} , shown as a thick dashed line, over time. A uniform planetesimal radius of 10 km is assumed.

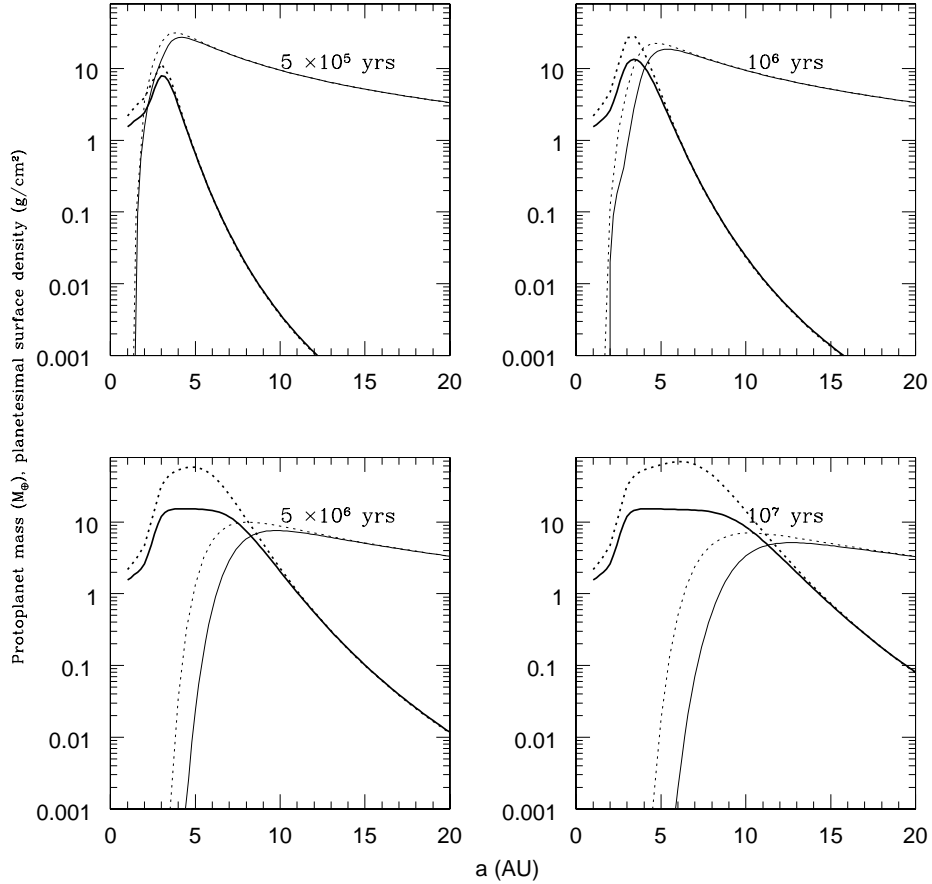


Fig. 4.— Protoplanet mass (thick curves) and planetesimal surface density (thin curves) versus heliocentric distance for a nebula with 10 times the solids and gas densities of the minimum-mass nebula. All other parameters are the same as for the minimum-mass case shown in Fig. 3. The dashed curves show the migration-less solution computed from Eqs. 20 and 24, while the solid curves show the solution including planetesimal migration, obtained from numerically integrating Eqs. 11 and 29.

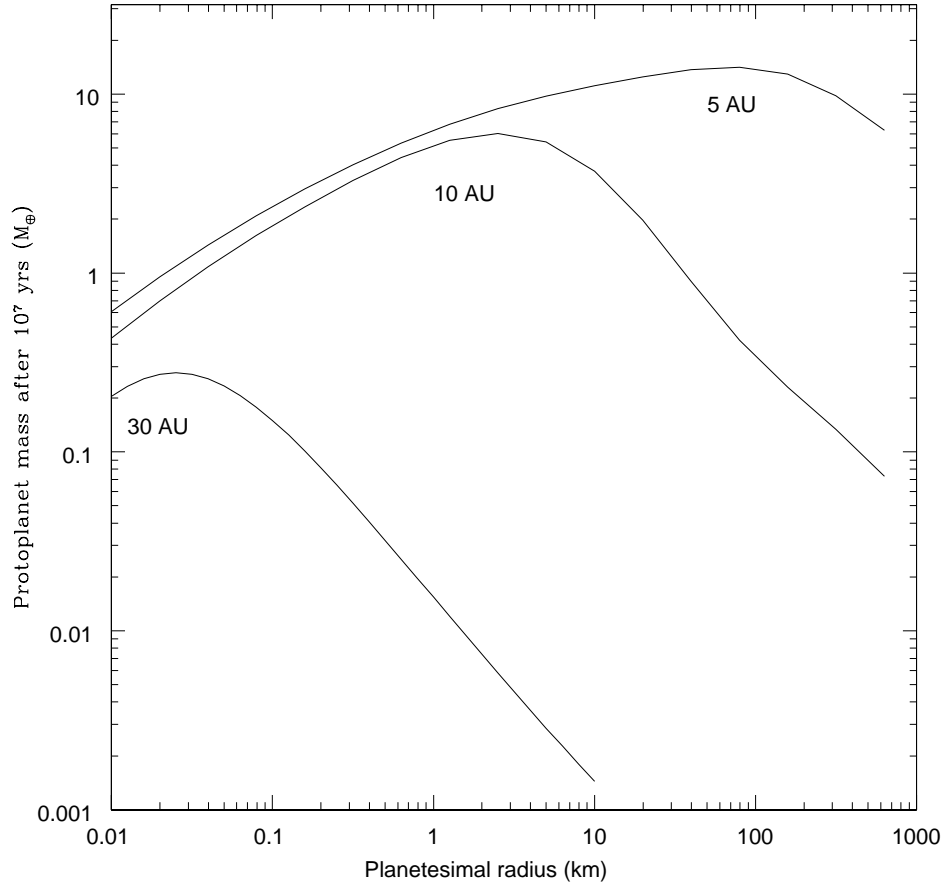


Fig. 5.— The largest protoplanet mass after 10 Myrs of oligarchic growth as a function of planetesimal radius at 5, 10 and 30 AU, in a $10\times$ minimum-mass disk. As can be seen, the optimal planetesimal radius r_m^{crit} is about 80 km, 2 km and 20 m, respectively.

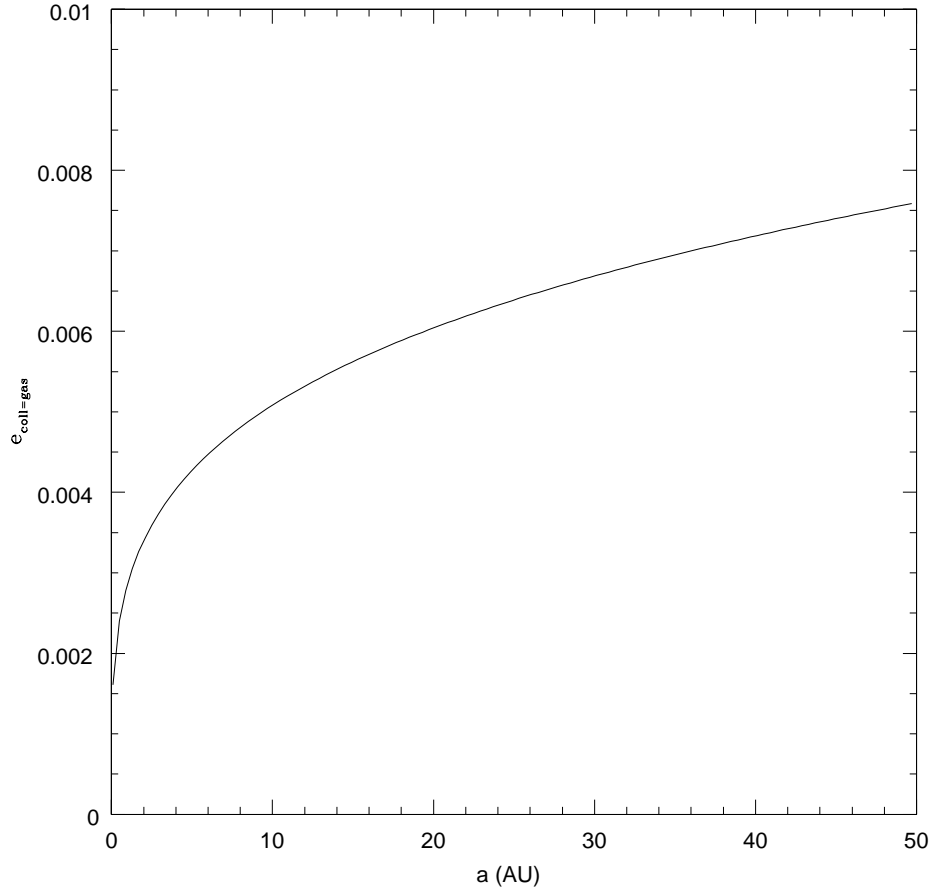


Fig. 6.— For a Hayashi-profile disk, the eccentricity $e_{\text{coll=gas}}$ at which the timescale for random velocity damping by gas drag comes to be equal to the planetesimal-planetesimal collision time. At higher eccentricities, the gas timescale is shorter.

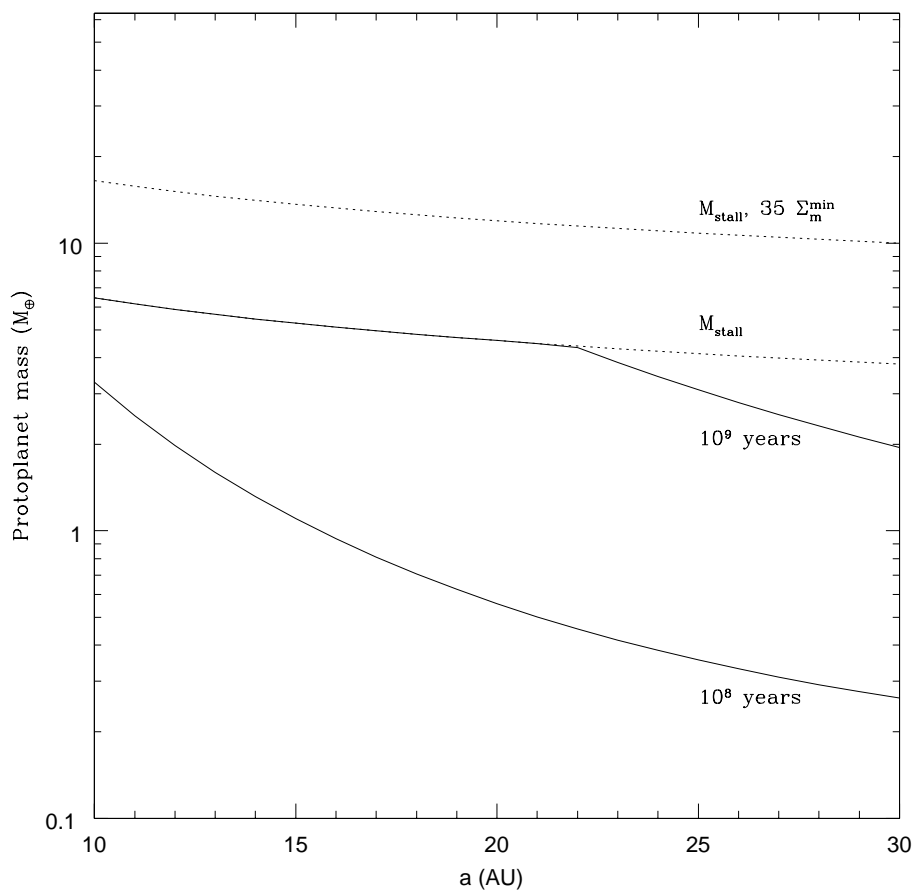


Fig. 7.— Protoplanet mass versus semimajor axis after 10^8 and 10^9 years of post-gas dispersal accretion, in a disk having ten times the solids surface density of the minimum-mass nebula. The lower of the dashed curves shows M_{stall} , the protoplanet mass at which significant escape of planetesimals likely terminates accretion. The upper dashed curve shows M_{stall} for a $35\times$ minimum-mass disk.

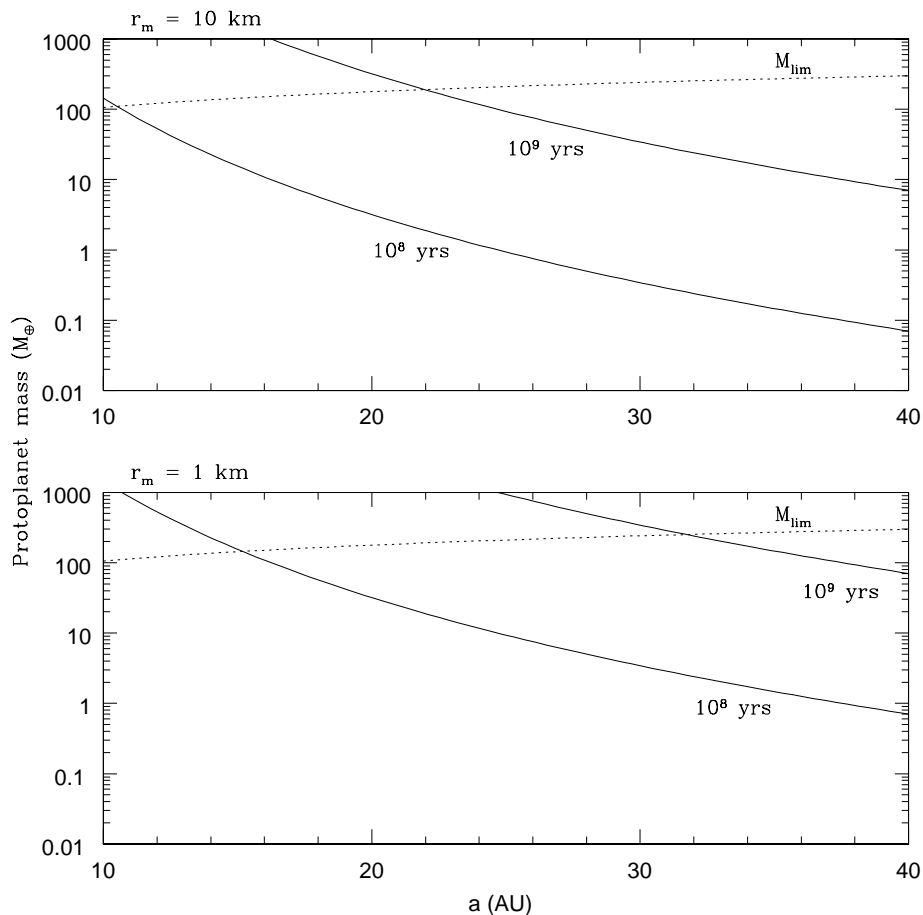


Fig. 8.— The protoplanet mass at 10^8 and 10^9 years, in the limit of maximally effective collisional damping of planetesimal random velocities. The dashed curve shows the limiting mass (Eq. 21), which is simply the mass at which a protoplanet has accreted all solids in an annulus of width $10 r_H$. The top panel shows the results for 10 km planetesimals, while the bottom panel shows the 1 km case; $M \propto 1/r_m$ so in the latter case the masses are simply scaled up by a factor of ten.

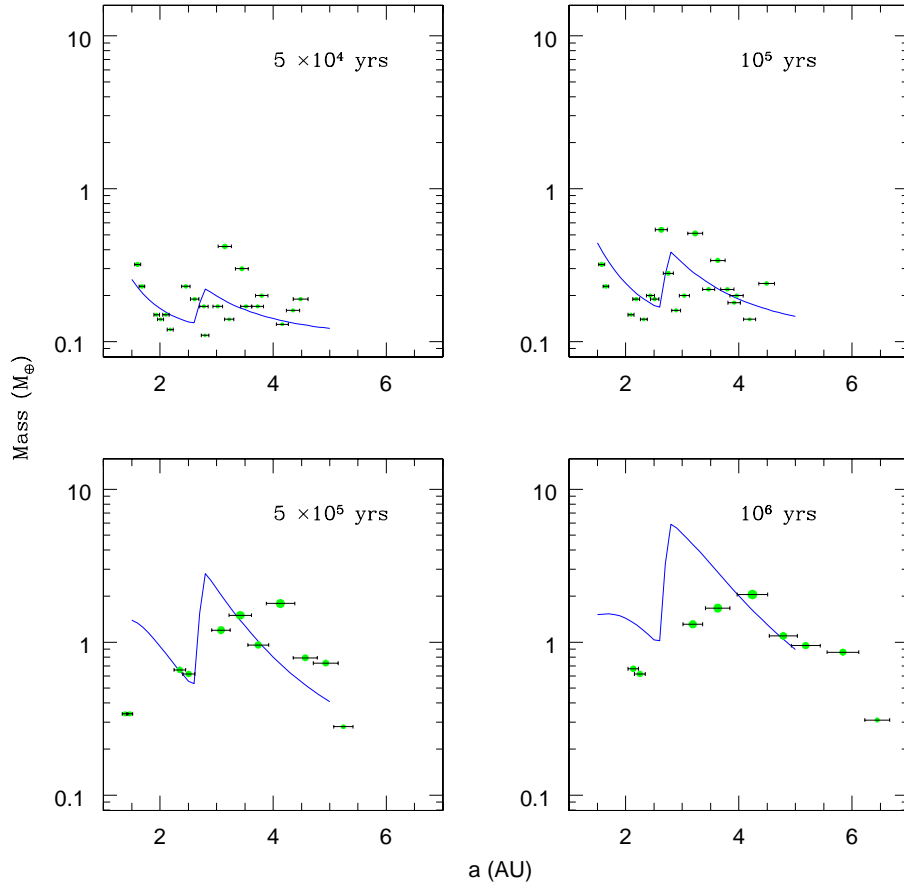


Fig. 9.— Snapshots of the protoplanet masses and semimajor axes in Run A at different times. The superimposed curve shows the mass predicted by the oligarchic growth model at each time, and the horizontal “error bars” on each protoplanet have a length of 10 Hill radii.

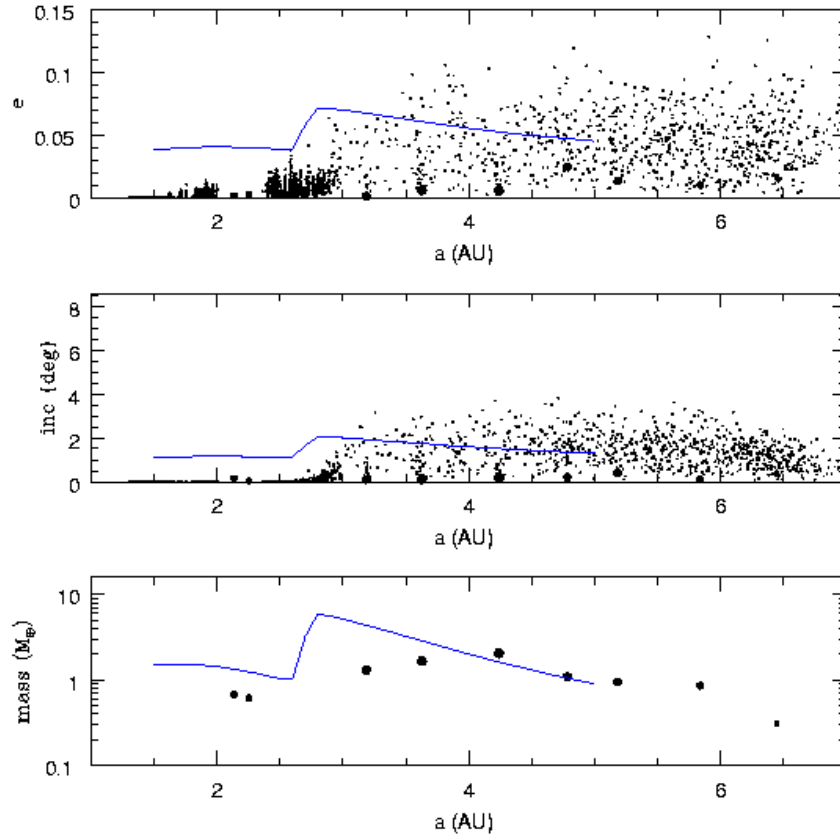


Fig. 10.— A more detailed snapshot of the state of Run A at its endpoint of 1 Myr, showing also the planetesimals. Eccentricities (top), inclinations (middle), and protoplanet masses are plotted versus semimajor axis, with superimposed curves showing their model-predicted values.

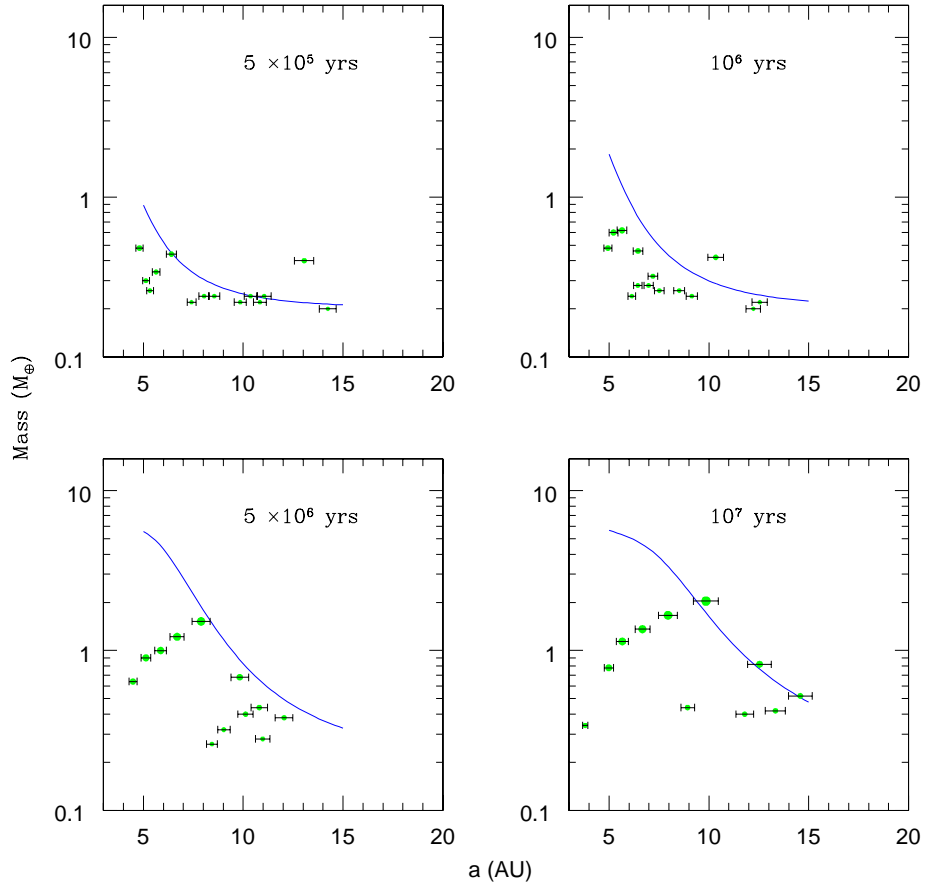


Fig. 11.— Snapshots of the protoplanet masses and semimajor axes in Run B at different times, together with the model-predicted mass function. The horizontal bars on the protoplanets are of length $10 r_H$.

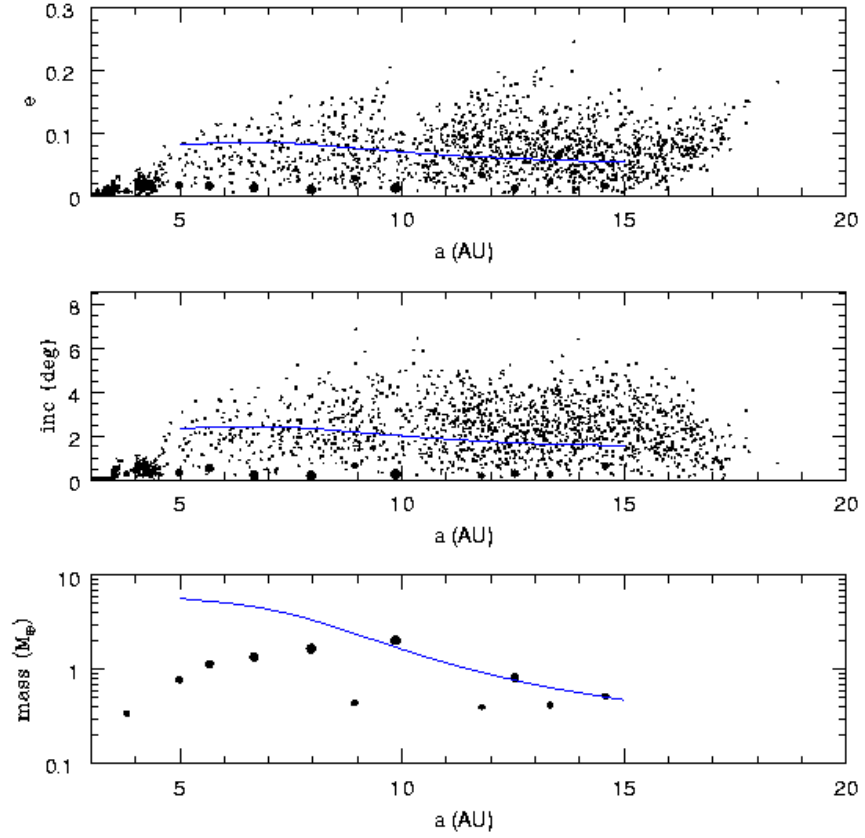


Fig. 12.— A more detailed snapshot of the state of Run B at its endpoint of 10 Myrs, showing eccentricities (top), inclinations (middle) and protoplanet masses (bottom) together with their predicted values.

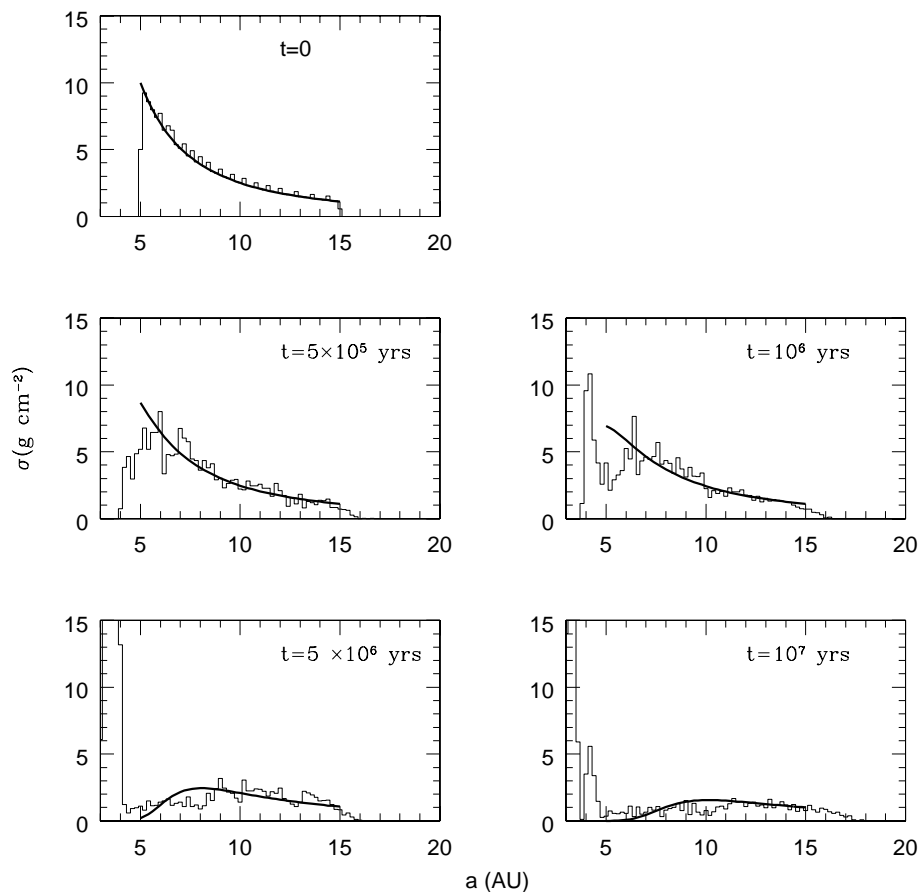


Fig. 13.— Evolution of the planetesimal disk surface density in Run B (histograms), revealing simulation edge artifacts. The superimposed curves show the model-predicted surface densities. By about a million years, the planetesimal surface density in the simulation falls well short of the theoretical value near the inner edge of the protoplanet population at 5 AU; by 10 Myrs, the underdense region has moved all the way out to ~ 11 AU. At the same time, inward-migrating planetesimals pile up interior to the protoplanets, leading to locally very high surface densities.

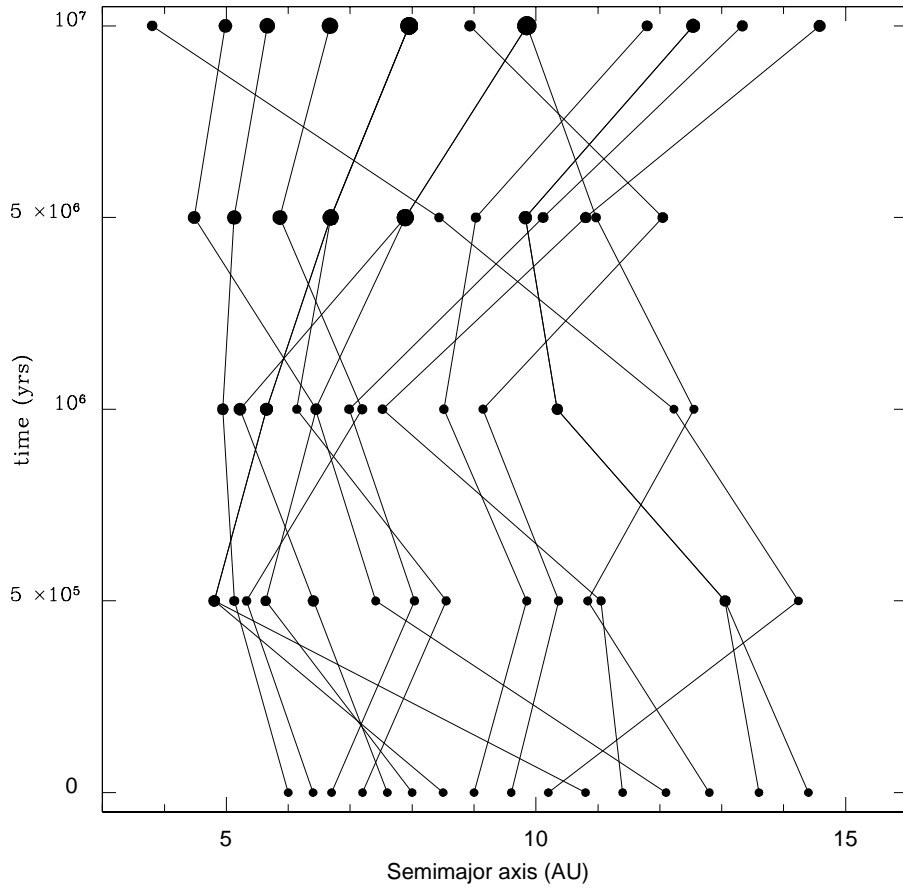


Fig. 14.— Evolution of protoplanet semimajor axes in Run B. The plotted circles are proportional to the protoplanets’ physical sizes. The connecting lines trace the history of each protoplanet. Going from bottom up, wherever multiple lines go in and one line comes out of a protoplanet, mergers have occurred in the intervening time; there are five mergers over the course of this run (note that there are no mergers at 10^6 yrs, only two protoplanets with nearly the same semimajor axis, about 6.5 AU)

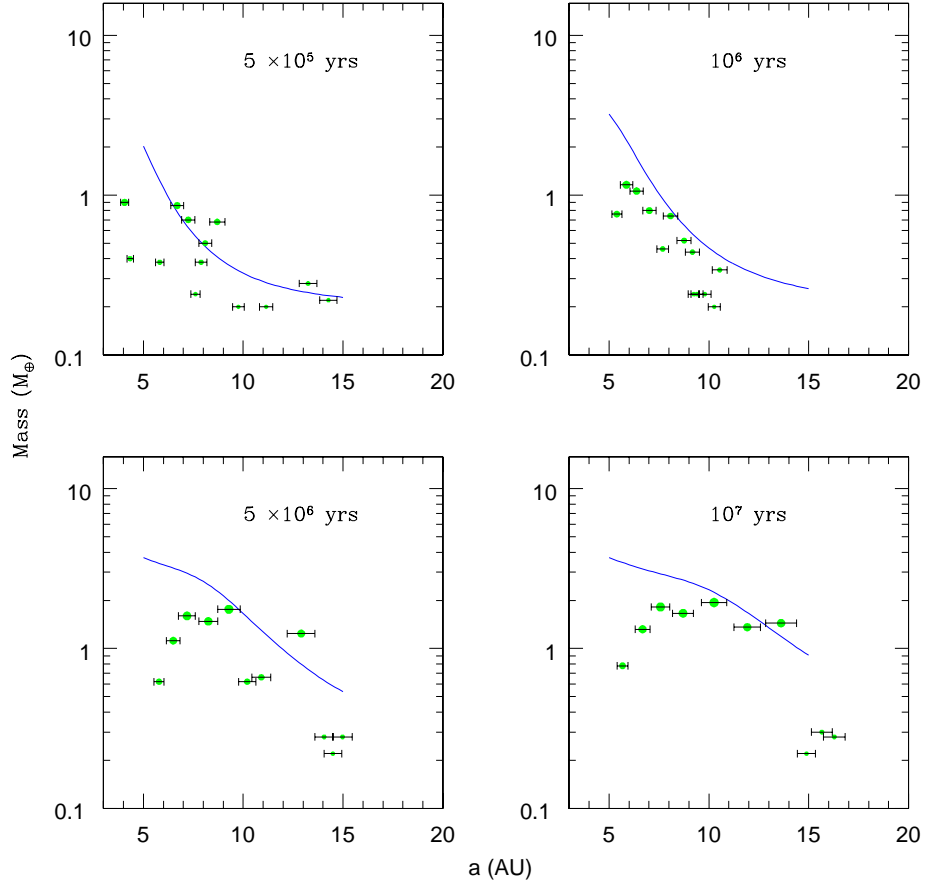


Fig. 15.— Snapshots of the protoplanet masses and semimajor axes in Run C at different times, together with the model-predicted mass function. The horizontal bars on the protoplanets are of length $10 r_H$.

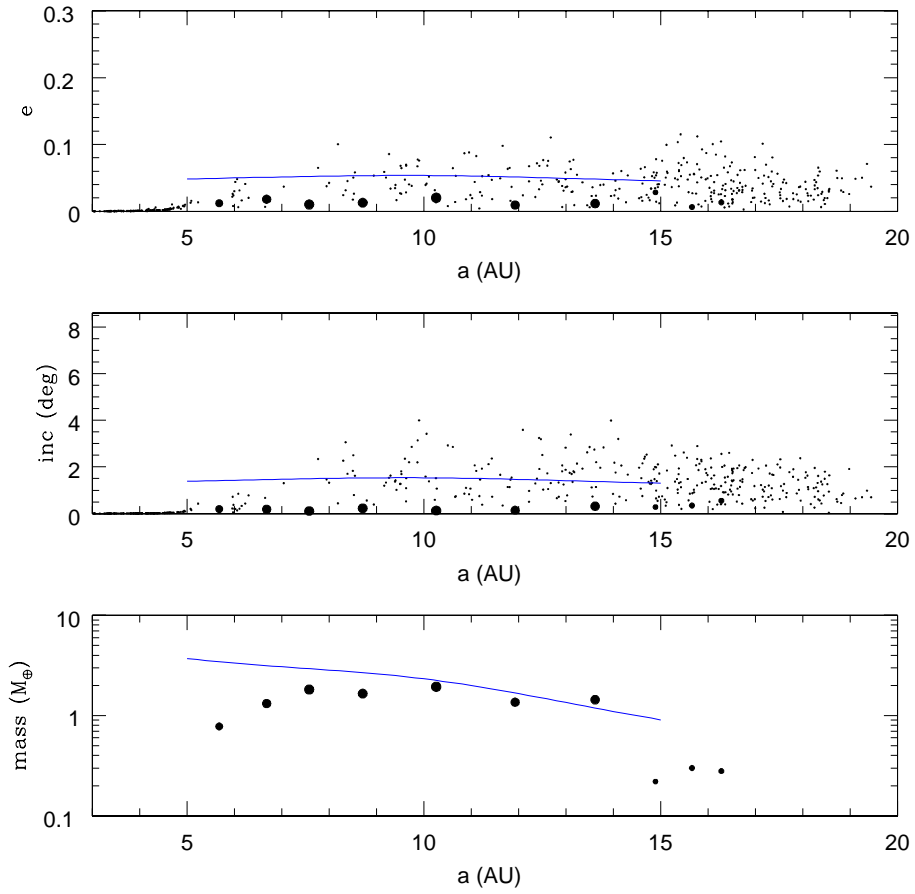


Fig. 16.— The state of Run C at its endpoint of 10 Myrs, showing eccentricities (top), inclinations (middle) and protoplanet masses (bottom) together with their predicted values.

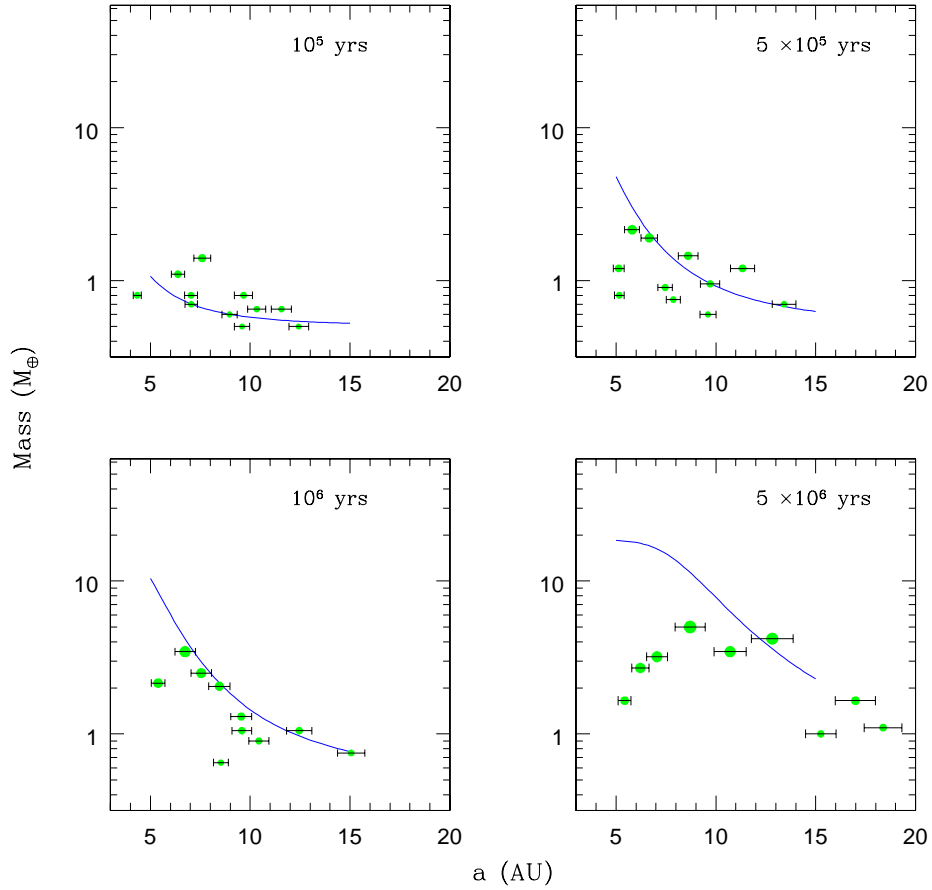


Fig. 17.— Snapshots of the protoplanet masses and semimajor axes in Run D at different times, together with the model-predicted mass. The horizontal bars on the protoplanets are of length $10 r_H$.

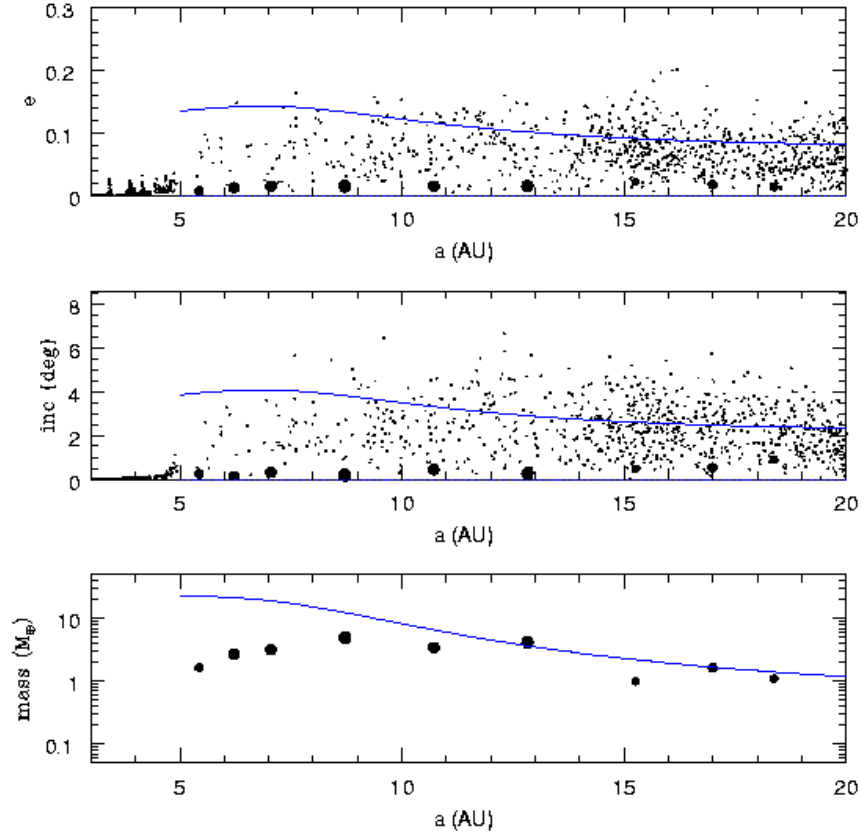


Fig. 18.— The state of Run D at its endpoint of 5 Myrs, showing eccentricities (top), inclinations (middle) and protoplanet masses (bottom) together with their predicted values.

Table 1: Simulation parameters

Quantity	Run A	Run B	Run C	Run D
initial solids surface density (g/cm ²)	$150 \left(\frac{a}{1 \text{ AU}}\right)^{-3/2}$	$250 \left(\frac{a}{1 \text{ AU}}\right)^{-2}$	$250 \left(\frac{a}{1 \text{ AU}}\right)^{-2}$	$225 \left(\frac{a}{1 \text{ AU}}\right)^{-3/2}$
gas volume density (10 ⁻⁹ g/cm ³)	$7 \left(\frac{a}{1 \text{ AU}}\right)^{-11/4}$	$11.5 \left(\frac{a}{1 \text{ AU}}\right)^{-13/4}$	$11.5 \left(\frac{a}{1 \text{ AU}}\right)^{-13/4}$	$10.5 \left(\frac{a}{1 \text{ AU}}\right)^{-11/4}$
initial radial extent	1.5 - 5	5 - 15	5 - 15	5 - 15
initial protoplanet mass (M _⊕)	0.1	0.2	0.2	0.5
initial protoplanet number	22	16	16	12
planetesimal mass	0.01	0.02	0.02	0.05
initial planetesimal number	4886	3233	3233	3446
planetesimal gas drag radius	10 km	10 km	1 km	10 km